8-2016

# A Savonius Wind Turbine with Electric Generator: Model and Test

Yogendra Kumar Yadav
*Clemson University*, yogendrakyadav89@gmail.com

# A SAVONIUS WIND TURBINE WITH ELECTRIC GENERATOR: MODEL AND TEST

---

A Thesis
Presented to
the Graduate School of
Clemson University

---

In Partial Fulfillment
of the Requirements for the Degree
Master of Science
Mechanical Engineering

---

by
Yogendra Kumar Yadav
August 2016

---

Accepted by:
Dr. John R. Wagner, Committee Chair
Dr. Todd Schweisinger, Committee Member
Dr. Yue Wang, Committee Member

# ABSTRACT

The overall goal of this research is to study the performance of Savonius wind turbine. Some of the advantages of a Savonius wind turbine include simple construction, good startup characteristics, low noise, and reduced wear. The applications of this type of wind machine include water pumping and small scale electricity generation. In the present research, an experimental model of the Savonius wind turbine is studied including the formulation of a mathematical model. The mathematic model for the torque acting on the Savonius rotor has been developed and the permanent magnet synchronous generator (PMSG) model has been simulated using the d-q synchronous reference frame theory.

In the present research, the mathematic model of the wind turbine system has been simulated in MATLAB/Simulink environment. The model includes the wind turbine model and the permanent magnet synchronous generator (PMSG) model. The wind turbine parameters of the experimental system have been used for the simulation purpose. A 1kW PMSG has been coupled with the wind turbine to study the dynamic performance of the wind turbine system. The system response and performance have been evaluated at 3 different wind speeds of 16.9 m/sec, 19.8 m/sec, and 21.9 m/sec corresponding to the wind speeds of the blower used for experimental system.

The experimental Savonius wind turbine has been developed to compare the numerical and experimental results. The experimental system includes Savonius rotor, PMSG, charge controller and rectifier, current and voltage transducers, frequency to analog converters, electrical load, and a National Instruments Data Acquisition Device (NI DAQ). The current and voltage transducers are used to measure the current and voltage in the

system and the outputs are connected to the NI DAQ. The frequency to analog converters are used to measure the rpm of the rotor and the anemometer. The charge controller is meant for battery charging applications of the system.

The numerical and experimental results have been obtained at three different wind speeds (16.9 m/sec, 19.8 m/sec, and 21.9 m/sec). The maximum value of the electric power generated is 2.7 Watts at a wind speed of 21.9 m/sec. Comparison of experimental and numerical results at the wind speed of 21.9 m/sec shows there is an approximate difference of 16%, 11%, 61% and 4% for the angular velocity, voltage, current, and electrical power generated, respectively. The difference in the values may be attributed to the fact that the mathematical model does not include the three-dimensional (3D) fluid effects and environmental factors.

# DEDICATION

This thesis is dedicated to my parents, friends, and family. Their support and love has provided me the motivation needed to finish this thesis. Without my family, I would not have had this wonderful opportunity for higher education.

# ACKNOWLEDGMENTS

I would like to thank my advisor Dr. John Wagner and my committee members, Dr. Todd Schweisinger and Dr. Yue Wang. I am also thankful of Mr. Michael Justice, and Mr. Jamie Cole from the Mechanical Engineering machine shop for their help designing and fabricating the experimental apparatus. Their patience, advice, and criticism have helped me mature not only as a student but also in life. They believed in my ability when I often doubted myself. They have taught me to be creative, think deeper, and strive to understand engineering subjects at a deeper level.

TABLE OF CONTENTS

Table of Contents (Continued)

Page

LIST OF TABLES

LIST OF FIGURES

List of Figures (Continued)

List of Figures (Continued)

List of Figures (Continued)

Figure Page

NOMENCLATURE LIST

| Symbol | Unit | Description |
|---|---|---|
| A | $m^2$ | Swept area |
| B | – | Damping coefficient |
| $C_d$ | – | Coefficient of drag |
| $C_{dD}$ | – | Coefficient of drag for advancing blade |
| $C_{dM}$ | – | Coefficient of drag for retreating blade |
| $C_p$ | – | Coefficient of power |
| $C_t$ | – | Coefficient of torque |
| D | m | Rotor diameter |
| $D_o$ | m | End plate diameter |
| e | m | Overlap distance between turbine blades |
| F | N | Force |
| $F_w$ | N | Wind force |
| H | m | Rotor height |
| $I_{base}$ | A | Base current |
| $i_{ds}$ | pu | d-axis stator current |
| $i_{qs}$ | pu | q-axis stator current |
| $i_s$ | pu | Magnitude of stator current |
| J | $kg.m^2$ | Moment of inertia of rotor |
| $J_g$ | $kg.m^2$ | Moment of inertia of generator |
| $L_{base}$ | mH | Base inductance |
| $L_d$, $L_q$ | | d- and q-axis inductance |
| n | m | Number of blades |
| P | - | Number of pole pairs |
| $P_{active}$ | W | Active electrical power generated |
| $P_t$ | W | Turbine power |
| $P_{total}$ | W | Total electrical power |
| $P_w$ | W | Wind power |
| r | m | Bucket radius |
| R | m | Rotor radius |
| $R_l$ | Ohm | Load resistance |
| $R_s$ | pu | Stator resistance |

| | | |
|---|---|---|
| $T$ | Nm | Torque |
| $T_{base}$ | Nm | Rated Torque |
| $t_p$ | m | End plate thickness |
| $t_t$ | m | Blade thickness |
| $T_e$ | pu | Electromagnetic torque |
| $T_m$ | pu | Mechanical torque |
| $T_{total}$ | Nm | Total torque |
| $u_{rotor}$ | m/s | Velocity of rotor |
| $u_\infty$ | m/s | Free stream velocity |
| $V_{base} = V_{L-L}$ | V | Line-Line base voltage |
| $v_{ds}$ | pu | d-axis stator voltage |
| $v_{qs}$ | pu | q-axis stator voltage |
| $V_s$ | pu | Magnitude of stator voltage |
| $x_a$, $x_b$, $x_c$ | - | a-, b- and c- axis components of space vector $\boldsymbol{x}$ |
| $x_d$, $x_q$ | - | d- and q-axis components of space vector $\boldsymbol{x}$ |
| $Z_{base}$ | ohms | Base impedance |
| $\phi$ | rad | Angle of attack |
| $\rho$ | $kg/m^3$ | Free stream density |
| $\omega$ | rad/s | Angular velocity |
| $\omega_{base}$ | rad/s | Rated speed |
| $\omega_r$ | pu | Rotor electrical angular speed |
| $\alpha$ | m | Angular acceleration |
| $\lambda$ | m | Tip speed ratio |
| $\lambda_r$ | pu | Rotor flux linkage |
| $\theta$ | rad | Angle subtended at turbine rotor center |
| $\eta g_{en}$ | - | Generator efficiency |
| $\eta_{mech}$ | - | Mechanical efficiency |

# CHAPTER ONE

# INTRODUCTION

A brief overview of the energy crisis and how renewable energy sources are a solution to this global problem will be presented in this chapter. The chapter also provides some data on the energy usage and the potential for energy that can be produced by renewable energy sources. Finally, a brief introduction on Savonius wind turbine and the past investigations on the wind turbine under study in this thesis will be offered.

## Renewable Energy

The long term energy crisis is one of the biggest issues of this century that needs to be tackled to ensure a prosperous future for coming generations. The consumption rate of the non-renewable sources of energy such as oil, natural gas and coal for the year 2014 was 92.086 Million barrels/day, 3393 Billion cubic meters, and 3881.8 Million tonnes oil equivalent, respectively to cater to the energy requirements of the public and private sectors (*Source: BP Statistical Review of World Energy,* June 2015). The non-renewable sources of energy are the fossil fuels such as coal, petroleum, and natural gas that were formed in the earth's crust over a span of millions of years. These fossil fuels are a combination of carbon compounds that have a very high specific energy which makes them suitable for energy needs across the globe. The use of fossil fuels increases the level of carbon dioxide, $CO_2$, in the atmosphere accompanied by the other pollutants including carbon monoxide, CO, and nitrous oxides, $NO_x$. The increase in the level of $CO_2$ impacts the greenhouse

effect, the process responsible for keeping heat locked in the earth's atmosphere. The imbalance caused in the greenhouse effect has resulted in global warning leading to increase in earth's temperature and other unfavorable changes. The world energy usage for the year 2014 is shown in Figure 1.1.

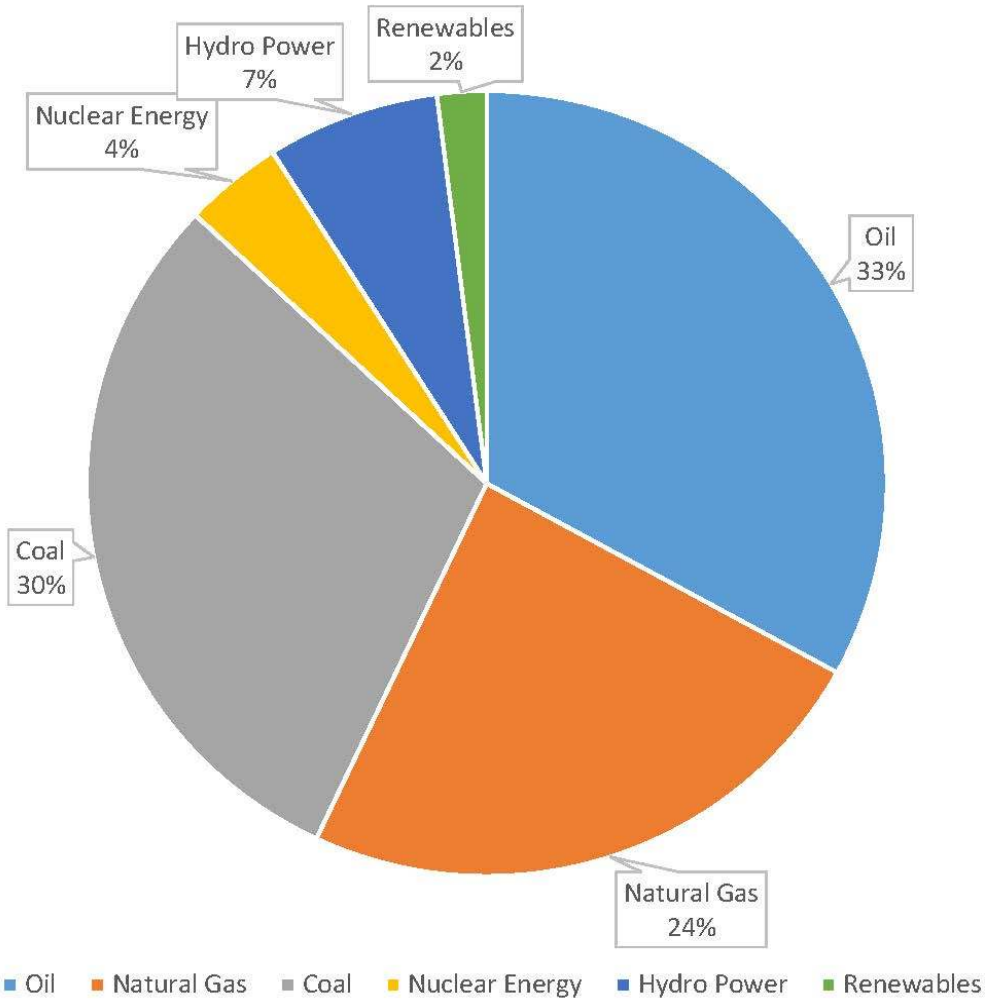


Figure 1.1: World Energy Consumption 2014, (BP Statistical Review of World Energy, 2015).

To deal with the energy crisis, the most promising solution is the use of renewable sources of energy. These include wind energy, solar energy, geothermal energy, tidal energy, biofuel, biomass, and hydro power. Another solution to the problem is the usage of regenerative power supplies (Ali *et al.*, 2015). Countries across the world have been trying to tap these resources and extensive research is being done on how to utilize these resources efficiently. Since the renewable sources of energy are inexhaustible, efforts need to be made in order to exploit these energy sources as much as possible. Out of these energy sources, wind and solar energy are the most promising sources of energy that can certainly help in dealing with energy crisis and help in restoring the earth's greenhouse effect balance (Cultura II and Salameh, 2011).

## Wind Energy

Wind energy is the kinetic energy stored in the wind. Heating of the earth's atmosphere by the sun and earth's rotation are responsible for causing the winds to flow.

Table 1.1: Wind Energy Production in 2015 (Global Wind Energy Council, 2015).

| Country | Capacity in 2015 (MW) |
|---|---|
| China | 145,104 |
| United States | 74,471 |
| Germany | 44,947 |
| India | 25,088 |
| Spain | 23,025 |
| United Kingdom | 13,603 |
| Canada | 11,200 |
| France | 10,358 |
| Italy | 8,958 |
| Brazil | 8,715 |
| Rest of the world | 66,951 |

According to a survey in 2006, the potential for wind energy production across the world was 686.1 PWh (Lu *et al.,* 2009). Since then every country has been trying to focus on the wind energy production to match up to the energy needs. Wind energy is also the world's fastest growing industry in electricity generation (Rahman *et al.*, 2009). From Figure 1.2 and Table 1.1, the total wind energy produced across different countries add upto 432,420 MW which is avery less portion of the potential energy. If the potential capacity is reached, then the energy crisis can be dealt with very easily.

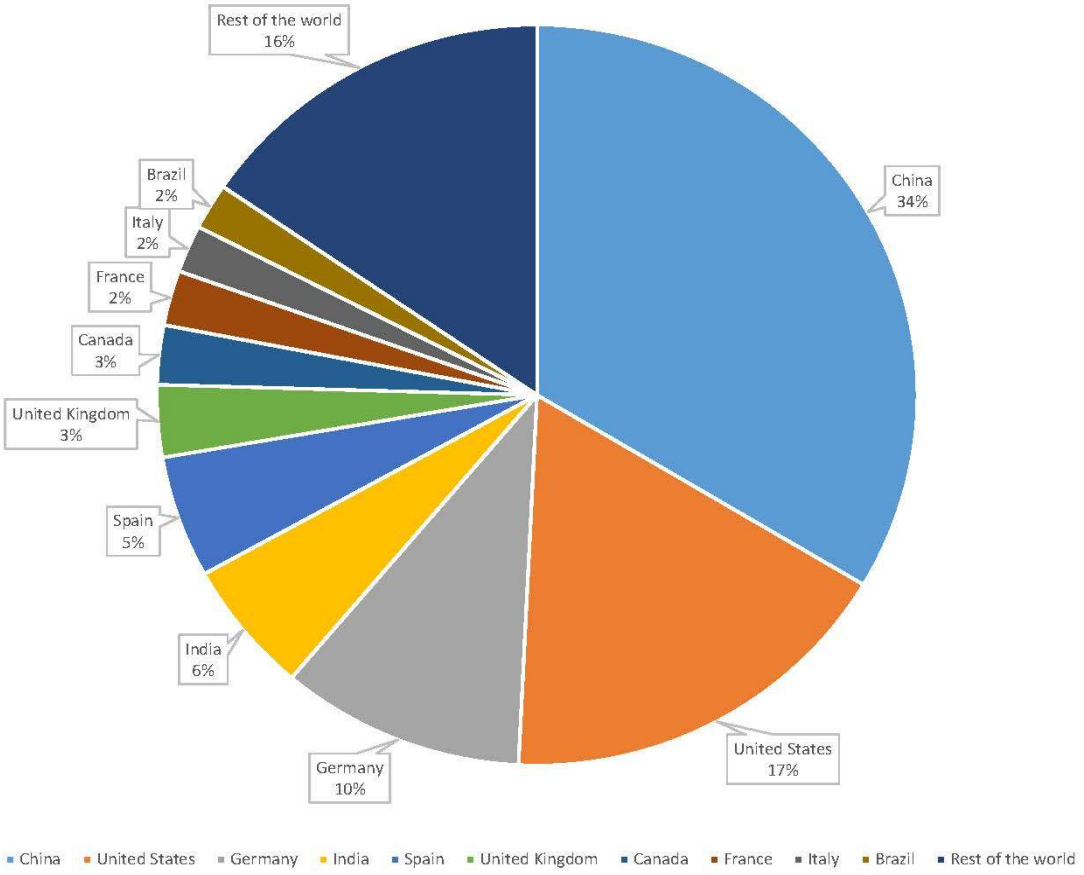


Figure 1.2: Cumulative Wind Energy Production Capacity of the World – 2015 (Global Wind Energy Council, 2015).

## History of Wind Turbines

The use of wind energy dates back to 5,000 BC for propelling the boats across the Nile River (*Wind Energy Foundation*). The Persians and Chinese utilized wind power for pumping water and grinding grains during 200 BC (*Wind Energy Foundation*). With the improvements in technology, new uses of wind power realized in the 11$^{th}$ century. The Dutch used it for pumping out water of the lakes by making certain changes to the wind mill configuration. By the 19$^{th}$ century, wind power was used for generating electric power. Wind mills existed in European countries, especially in Denmark until the 1950s, when they were edged out due to the cheap oil and energy prices (*Wind Energy Foundation*). In 1970s due to the fear of oil shortage in the US, extensive research was done to improve the wind turbine technology. Since then, the government has been encouraging the use of renewable energy sources to avoid potential energy crisis. The present day wind turbine technology has improved a lot in terms of efficiency, ease of operation, and price.

## Types of Wind Turbines

The wind turbines can be broadly classified in to two categories, Horizontal axis (HAWT) and Vertical axis (VAWT) in accordance with the alignment of the axis of rotation of the rotor with respect to the ground. The horizontal axis (HAWTS) wind turbines have their axis of rotation parallel to the ground and the vertical axis (VAWTs) wind turbines have their axis of rotation perpendicular to the ground. The wind turbines can also be categorized on the basis of the major force responsible for rotation, i.e., lift force or drag force. In this section we will give a brief overview of the HAWTs and VAWTs.

The horizontal axis (HAWT) wind turbine is an improved version of the old wind mill where the propeller is made up of blades and spins in the horizontal axis and hence the name, horizontal axis. The main rotor shaft and the electric generator are placed on top of the tower. All the mechanical systems including the gearbox, motors, etc. are packed inside a metal cover called the nacelle. The HAWT should always be pointed towards the wind direction so, a wind sensor along with a servo motor is used to move the turbine rotor in the wind direction. A gearbox is coupled between the rotor shaft and the generator shaft in order to turn the generator shaft at much higher speed than the rotor shaft for efficient production of electricity. Some of the advantages include; the tall tower provides access to stronger winds, and very high efficiency in comparison to other types of wind turbines. The disadvantages include: a strong tower is required to support the massive components, it's difficult to raise the heavy components to such a height, and these require additional yawing and braking mechanisms. These extra mechanisms including the gearbox make the wind turbine heavier and also expensive. The height also makes maintenance difficult.

In case of a vertical axis (VAWT) wind turbine, the rotor shaft is placed perpendicular to the ground. This type of configuration does not require any heavy tower so, the generator and other important components can be placed close to the ground. Due to the vertical configuration, the VAWTs don't have to be face the wind direction at all times. The two most famous horizontal axis wind turbines are the Darrieus wind turbine and the Savonius wind turbine.

Some of the advantages of vertical axis configuration are: no yawing mechanism required, light, cheap and easy to maintain, lower start up speeds, and can be installed on

rooftops of buildings and houses. The VAWTs have some disadvantages they are as follows: reduced efficiency due to drag forces, and due to lower height, they cannot utilize the strong winds.

Figure 1.3: Typical Horizontal Axis Wind Turbine ((Golden, Colorado); courtesy of DOE/NREL, credit – Dennis Schroeder, PIK # 25907)
www.nrel.gov.

Figure 1.4: Savonius and Darrieus Wind Turbines.

Savonius Wind Turbine

Savonius wind turbine is a drag based vertical axis wind turbine. It was invented by a Finnish engineer S.J. Savonius in the year 1922. It is one of the simplest types of wind turbine with the rotor made up of two or three scoops. The top view of a conventional Savonius rotor looks like an ‘S’ shape. When the air hits any of the scoops, a pressure differential is created across the surface of each scoop which results in a drag force that makes the rotor spin.

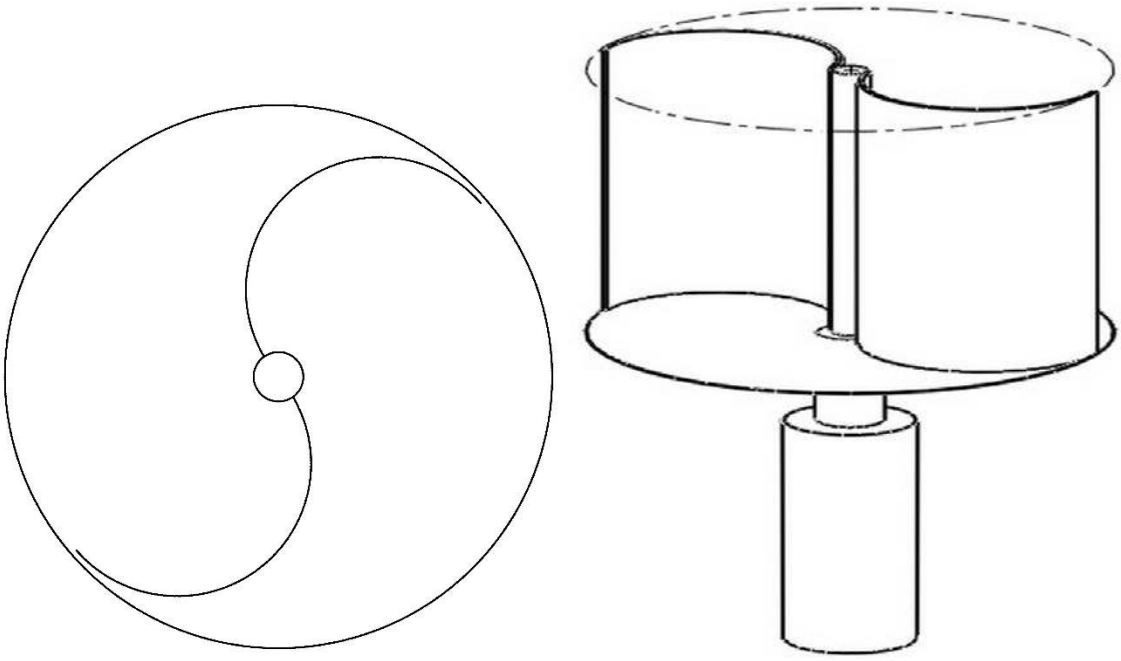

Figure 1.5: Top and Front View of a Savonius Wind Turbine.

## Related Work

Researchers have been exploring methods to improve the starting characteristics of the Savonius rotor and investigating the feasibility of Savonius wind turbine for power generation. Hayashi *et al.* (2005) designed a three stage Savonius rotor with a 120-degree bucket phase shift between adjacent stages. Khan (1978) tested a similar design with a two stage rotor with a 90-degree phase shift. The three stage and two stage rotors slightly improved the starting characteristics by reducing the torque variation and range of negative starting torque. Another effort to improve the starting characteristics of the Savonius rotor was made by Ali (2013) by comparing a conventional two blade rotor and a three blade rotor. The results show that the two blade rotor is more efficient than the three blade rotor, reason being the increase in number of blades increases the negative torque significantly

due to increased projected area. Kamoji *et al.* (2008) tested single stage, two stage and three stage Savonius rotor with multiple aspect ratios. The study revealed a reduction in performance by increasing the number of stages, keeping the aspect ratio same. Saha *et al.* (2008) performed a similar study with semicircular and twisted blades. Multiple experiments were carried out to optimize parameters including number of stages, number of blades and geometry of blades. Farsaie *et al.* (1984) studied the performance of Savonius rotor in horizontal and vertical orientation with varying the pitch, angle of incidence and rotor position. Saha and Rajkumar (2006) have investigated a three blade rotor system with twisted blades. The experiments show an increase in the efficiency and self-starting capability, in comparison to the conventional rotor and also, the optimum angle of twist for maximum performance. Sharma *et al.* (2005) tested three designs of Savonius rotor with different material and overlap ratios. A detailed study has been performed by Akwa *et al.* (2012) on numerous possible configurations of the rotor including varying the bucket spacing, overlap, shape, profile, number and thickness. Performance gains of up to 50% were reported in the study. An extensive study was performed by Modi and Fernando (1989) on assessing the influence of different parameters on the Savonius rotor performance. The study reported a 100% increase in the efficiency by providing an optimum configuration. Reupke and Probert (1991) tested the conventional Savonius rotor with a rotor with

Past investigations on the Savonius rotor have been conducted using wind tunnel tests, field experiments, and numerical investigations utilizing commercial computational fluid dynamics software like FLUENT, ANSYS, etc. Hassan *et al.* (2010) presented a CFD analysis of a twisted Savonius rotor using Flow-3D software with a 180-degree twist in the

blade configuration. Deb *et al.* (2013) performed a similar analysis using FLUENT 6.2 with a 45-degree twist angle in the rotor blades. Another interesting analysis was performed by D'Alessandro *et al.* (2010) employing FLUENT coupled with MATLAB. The CFD data was imported to MATLAB and the angular velocity was calculated and then fed back to the CFD code. The mathematical model was validated by comparing the results with the Environmental Wind Tunnel Laboratory at Polytechnic University of Marche with their testing of a Savonius rotor. El-Aksary *et al.* (2015) analyzed three different designs of guide plates using FLUENT 6.3 for improving the performance of Savonius rotor. Fujisawa and Gotoh (1992) studied the pressure on the blade surface for investigating the power mechanism of a Savonius rotor. The study found a low pressure region on the convex side of the advancing blade that contributes to the power production. Altan and Atilgan (2008) performed a study for improving the performance of the Savonius rotor by designing a curtain for the convex side of the rotor. Studies show a considerable increase in the output by using the curtain. Wakui *et al.* (2005) tested two hybrid configurations of Darrieus and Savonius rotors. Results show that the configuration with Savonius rotor inside Darrieus rotor is an effective configuration for small scale systems.

## Learning Objectives

A series of student learning objectives in the undergraduate laboratory can be identified to consider when teaching about the general operation of a vertical axis Savonius wind turbine.

- Development of mathematical models for the different parts of the wind turbine system can provide insight into the aerodynamics and mechanics of the Savonius

rotor, as well as the dynamics of a permanent magnet synchronous generator (PMSG).

- Computer simulation of the integrated Savonius rotor and PMSG in the MATLAB/Simulink environment to study the behavior of the system under different wind speeds.
- Data collection using National Instruments (NI) based on the experimental Savonius wind turbine introduces sensors and actuators. A virtual instrument (VI) is created in NI LabView software to process the test data.
- Comparisons between the experimental and numerical results can lead to suggested improvements in both the test platform and the mathematical model for greater power generation and more accurate results.
- Empowerment of students to design renewable energy systems for residential and commercial applications.

# CHAPTER TWO

# SAVONIUS WIND TURBINE: MODEL

## System Overview

The Savonius wind turbine is a vertical axis wind turbine which derives its power form drag force on its rotor surface. The conventional shape of a Savonius rotor is a "S-shape" that is created by two semi-circular buckets. The top view of the rotor is shown in Figure 2.1. The blades can be made out of plastic or aluminum sheets and bent into a semi-circular shape.

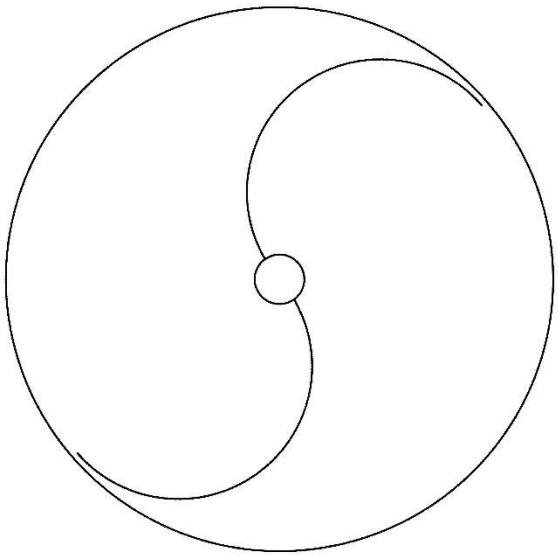

Figure 2.1: Top View of a Savonius Rotor with Characteristic "S" Shape.

A gearbox which takes the low rotational speed of the rotor shaft and increase it to the desired level, in order to get the generator to produce required power. The optimum gear ratio can be achieved by a combination of gears like planetary, helical, spur or worm gears.

The rotational mechanical energy of the turbine rotor is converted to electrical energy by the generator. The generator work on the Faraday's law of electromagnetic induction, according to which a conductor moving in a magnetic field produces an induced emf. Generators can be used to generate AC or DC current as the application requires.

## Dynamic Equations

A mathematical model for the Savonius rotor subject to an external wind with speed $u_{\infty,}$ will be derived to evaluate the torque acting on the rotor. A lumped parameter analysis allows application of Newton's and Kirchhoff's laws.

## Aerodynamics

Wind power is a function of the mass flow rate per unit time and the kinetic energy per unit area which is given by

$$P_w = \frac{1}{2}\rho A u_\infty^3 \tag{2.1}$$

The swept area $A = H * D$ is dependent on the rotor height, $H$, and the rotor diameter, $D$ (Hayashi *et al.*, 2005).

The tip speed ratio $\lambda$, is defined as the ratio of the peripheral velocity of the Savonius rotor to the free stream velocity so that

$$\lambda = \frac{u_{rotor}}{u_\infty} \tag{2.2}$$

The peripheral velocity of the Savonius rotor is the product of the angular velocity, $\omega$, and the rotor radius, $R$, such that $u_{rotor} = \omega R$.

The Savonius rotor torque is the product of the moment of inertia of the rotor and the angular acceleration of the rotor, or $T = J\alpha$ .

The efficiency of a wind turbine is measured by the amount of power harnessed by the wind turbine. The efficiency is measured by Coefficient of power, $C_p$, which is defined as the ratio of the power extracted by the wind turbine to the available wind power so that

$$C_p = \frac{P_t}{P_w} \tag{2.3}$$

Mechanics

The power extracted by the Savonius rotor is given by

$$P_t = T\omega \tag{2.4}$$

A mathematical model has been formulated using the basic definition of torque, $T$ = *Force* × *Distance*, to evaluate the power of a two-bucket Savonius rotor with zero over-lap ratio (e/D=0)(refer to Appendix B).

The total torque is given by

$$T = 2rF_w \int_0^{\pi/2} \cos\theta \sin(\theta+\phi) \mathrm{d}\theta \tag{2.5}$$

where $r$ is the bucket radius, $F_w$ is the wind force, respectively.

The wind force is given by

$$F_w = \frac{1}{2}\rho A u_\infty^2 C_d \tag{2.6}$$

where $A$ is the swept area of the rotor ($A=4rH$), $\rho$ is the free stream air density, $u_\infty$ is the

free stream velocity, and $C_d$ is the coefficient of drag. The coefficient of drag for the re-treating and the advancing blades are given by $C_{dM}$ and $C_{dD}$, respectively.

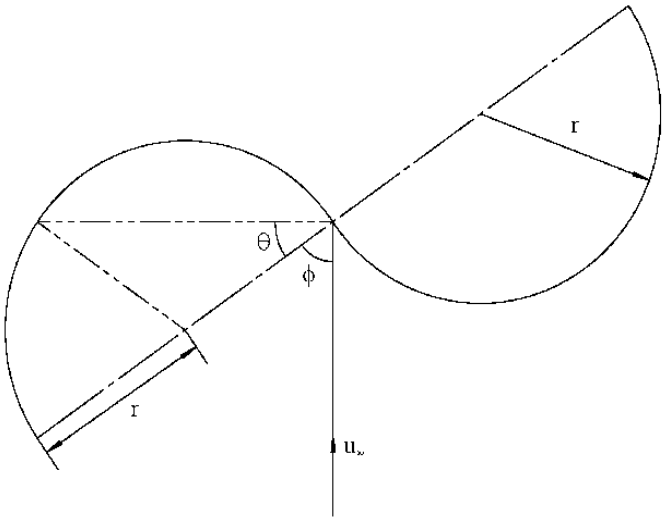


Figure 2.2: Savonius Rotor Schematic with Angle of Attack, $\phi$.

Using equations (2.5) and (2.6), the estimated mechanical torque, $T_m$, is

$$T_m = \eta_{mech}\left(\rho u_\infty^2 C_d\right)\int_0^{\pi/2}\left(r\cos\theta\right)\sin\left(\theta+\phi\right)d\theta \tag{2.7}$$

where $\phi$ is the angle of attack as can be seen in Figure 2.2 and $\eta_{mech}$ is the mechanical efficiency. From the above equation it can be concluded that the total torque is a function of the angle of attack which varies from 0 to 2π. According to the Newton's Law of Rotation, the net external torque is proportional to the angular acceleration. The rotation of the Savonius rotor is about a single principal axis therefore, the relation is given by

$$\sum T = T_{total} = J\alpha = J\frac{d\omega}{dt} \tag{2.8}$$

Using the above relation, the mechanical equation of the system is derived as

$$J\frac{d\omega}{dt} + B\omega = T_m - T_e \tag{2.9}$$

where $B$ is the generator damping coefficient, $J$ is the combined moment of inertia of the system and $T_e$ is the electromagnetic torque developed by the generator and is given by equation (2.11)(Ahmed *et al.*, 2013).

Generator (Permanent Magnet Synchronous Generator)

The voltage equations for a permanent magnet synchronous generator (PMSG) in the *dq*- frame are given by

$$\begin{aligned} v_{ds} &= -R_s i_{ds} + \omega_r L_q i_{qs} - L_d \frac{di_{ds}}{dt} \\ v_{qs} &= -R_s i_{qs} - \omega_r L_d i_{ds} + \omega_r \lambda_r - L_q \frac{di_{qs}}{dt} \end{aligned} \tag{2.10}$$

where $v_{ds}$ and $v_{qs}$ are d- and q- axis stator voltages, $i_{ds}$ and $i_{qs}$ are the d- and q-axis stator currents, $\omega_r$ is the generator shaft speed, $R_s$ is the stator resistance, $L_d$ and $L_q$ are the *d*- and *q*-axis inductances, and $\lambda_r$ is the rotor flux linkage (El-Saady *et al.*, 2013).

The electromagnetic torque developed can be calculated by

$$T_e = \frac{3P}{2}\left(i_{qs}\lambda_r - (L_d - L_q) i_{ds} i_{qs}\right) \tag{2.11}$$

where $P$ is the number of pole pairs of the generator (Khater *et al.*, 2014).

The generator mechanical speed, $\omega$, and the generator electrical speed, $\omega_r$, are related by the relationship

$$\omega_r = P\omega \tag{2.12}$$

CHAPTER THREE

# PERMANENT MAGNET SYNCHRONOUS GENERATOR

## Introduction

The conversion of mechanical energy of the wind turbine rotor into electrical energy is done using a generator coupled with the rotor shaft. For large applications, AC machines are used and for small applications DC machines are preferred. The right selection of generator is very important for wind turbine applications. Some of the factors that need to be considered include source, type of load, and speed of the wind turbine. The most popular types of generators in wind turbine applications are induction and synchronous generators are shown in Figure 3.1.

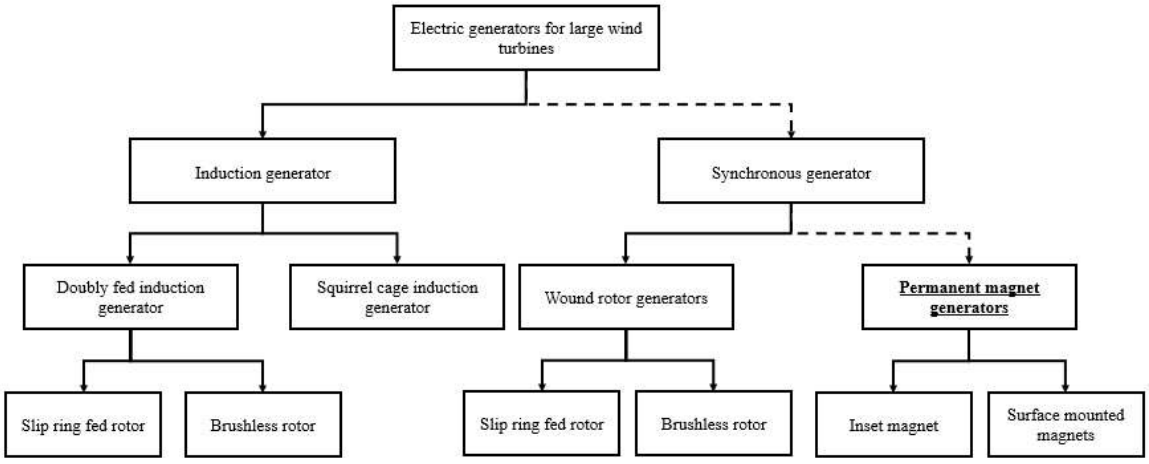


Figure 3.1: Commonly Used Electric Generators in Wind Turbine (Underlined block is the generator under investigation).

The induction machines (refer Figure 3.2) can work both as a motor and a generator depending on the speed of the rotor shaft. If the shaft rotates slower than the synchronous speed, the machines works as a motor and if the shaft rotates faster than the synchronous

speed, the machine works as a generator. The main advantage of an induction machines is its low cost and ease of availability. The disadvantages of an induction machine are: (1) Need external excitation to produce a rotating magnetic field,and (2) requires a gear-train which is responsible for noise and high maintenance.

Permanent magnet synchronous generators (refer Figure 3.2) do not require a gear-train and therefore are called direct driven generators (Sankar and Seyezhai, 2013). These generators are more efficient and reliable than the induction type generators (Badoni and Prakash, 2014). This is the main reason that these generators are used for small scale applications. The permanent magnet generators have multiple poles and therefore can directly be connected to the rotor shaft. These type of generators have become really popular recently because of the reduced price of the magnets, improved magnetic material properties, and reduced mass of the system (Yin *et al.*, 2007).

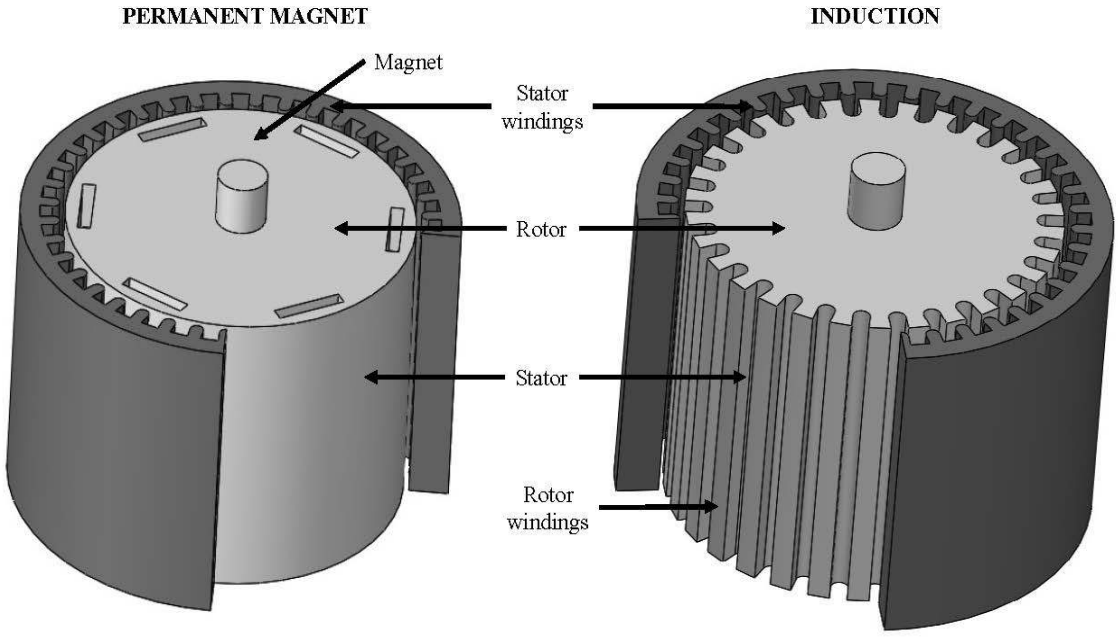


Figure 3.2: Permanent Magnet and Induction Type Machine Configuration.

In this research, the analysis of a permanent magnet synchronous generator coupled with a Savonius wind turbine is presented. The modelling of the wind turbine system and the generator is done in MATLAB/Simulink environment.

## Reference Frame Theory

The reference frame theory is a very useful tool in simplification of the analysis of electrical machines and implementation in various simulation environments. The complex three-phase AC circuits are simplified using the reference frame theory by reducing the number of variables in the system. Let us consider three-phase electrical variables, $x_a$, $x_b$, and $x_c$, which can represent either voltage, current, or flux linkage (El-Saady *et al.*, 2013). This system can be represented by a space vector $\vec{x}$ in the three-phase (*abc*) co-ordinate system. The space vector $\vec{x}$ rotates at an angular speed ω with respect to *abc* stationary frame (El-Saady *et al.*, 2013). The relationship between the space vector $\vec{x}$ and its three phase values $x_a$, $x_b$, and $x_c$ is shown in Figure 3.3.

The a, b, and c axes are $2\pi/3$ out of phase and are used to calculate the three phase values $x_a$, $x_b$, and $x_c$ by projecting $\vec{x}$ onto the corresponding axes. The magnitude of the $\vec{x}$ is assumed constant and hence the waveforms of $x_a$, $x_b$, and $x_c$ are sinusoidal with a phase shift of $2\pi/3$. To simplify the three-phase model calculations, the three-phase variables in *abc* frame are transformed into two-phase variables in *dq* (direct-quadrature) reference frame where the *d* and *q* axis are perpendicular to each other. An arbitrary position is assumed for the *dq*-axis with the *abc* reference frame so that the angle between *a*-axis and *d*-axis is $\theta$. The *dq*-frame rotates at an angular speed $\omega$; where $\omega = d\theta/dt$.

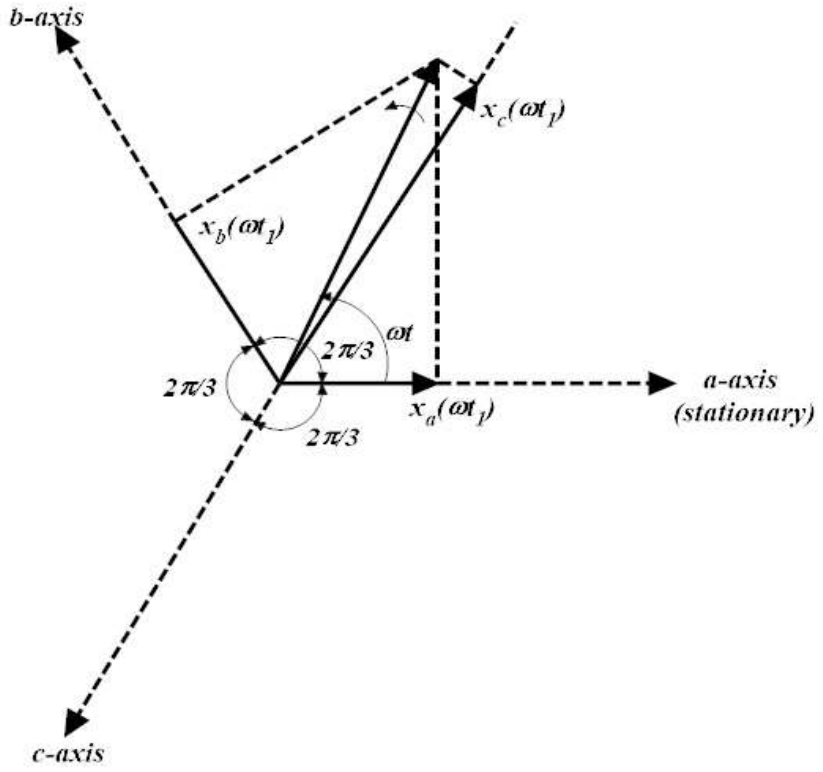


Figure 3.3: Space Vector $\vec{x}$ and its Three-phase Variables $x_a$, $x_b$, and $x_c$.

The transformation can be done by simply deriving the trigonometric functions of the orthogonal projections of $x_a$, $x_b$, and $x_c$ onto the *dq*-axis also known as Park's Transformation (Gupta and Kumar, 2015). The sum of all the d-axis and q-axis projections can be expressed in a matrix form as follows:

$$\begin{bmatrix} x_d \\ x_q \end{bmatrix} = \frac{2}{3} \begin{bmatrix} \cos\theta & \cos(\theta - 2\pi/3) & \cos(\theta - 4\pi/3) \\ \underbrace{-\sin\theta}_{A-axis} & \underbrace{-\sin(\theta - 2\pi/3)}_{B-axis} & \underbrace{-\sin(\theta - 4\pi/3)}_{C-axis} \end{bmatrix} \begin{bmatrix} x_a \\ x_b \\ x_c \end{bmatrix} \tag{3.1}$$

The transformed *dq* variables contain all the information of the *abc* variables provided the system is three-phase balanced. If two variables of a three-phase balanced system are known, the third one can be calculated by

$$x_a + x_b + x_c = 0 \tag{3.2}$$

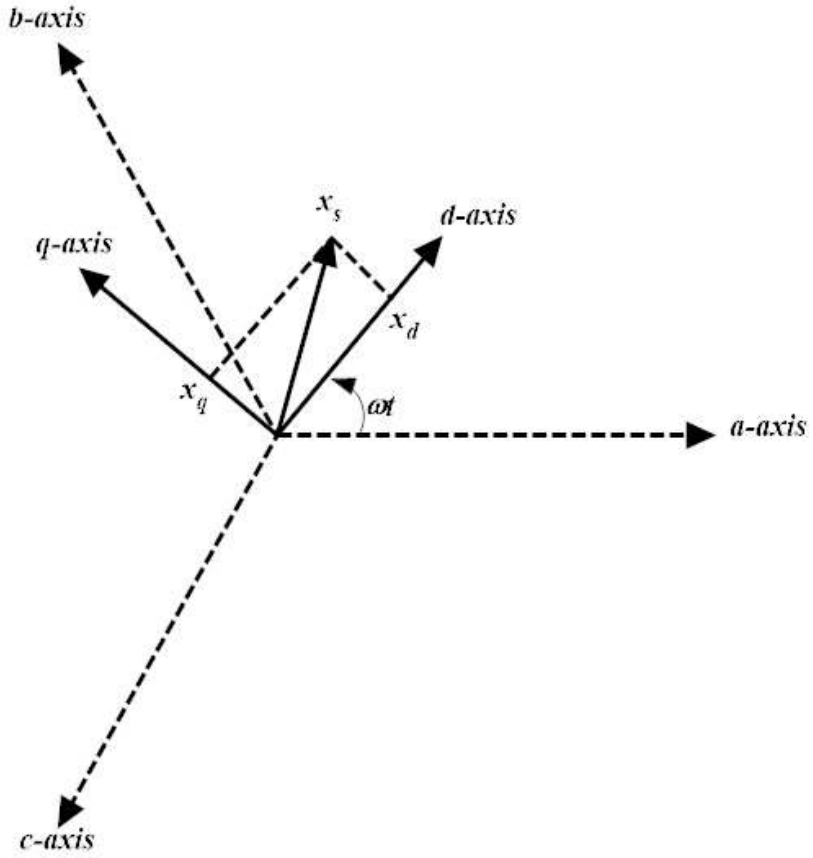


Figure 3.4: Transformation of Three-phase (*abc*) Variables into Two-phase (*dq*) Variables.

The *abc* variables can be derived from the *dq* variables by performing an inverse transformation on the matrix form equation (3.1) so that

$$\begin{bmatrix} x_a \\ x_b \\ x_c \end{bmatrix} = \begin{bmatrix} \cos\theta & -\sin\theta \\ \cos(\theta - 2\pi/3) & -\sin(\theta - 2\pi/3) \\ \cos(\theta - 4\pi/3) & -\sin(\theta - 4\pi/3) \end{bmatrix} \begin{bmatrix} x_d \\ x_q \end{bmatrix} \tag{3.3}$$

Dynamic Equations

The dynamic modeling of the PMSG is done using the equivalent circuits of the reduced *dq*-axis circuits (Weisgerber *et al.*, 1997). The reduced equivalent circuits of the *d*-axis and *q*-axis circuits in the rotor-field synchronous reference frame are shown below, is valid for both salient- and non-salient pole synchronous generators. The transformation can be done by simply deriving the trigonometric functions of the orthogonal projections of $x_a$, $x_b$, and $x_c$ onto the *dq*-axis.

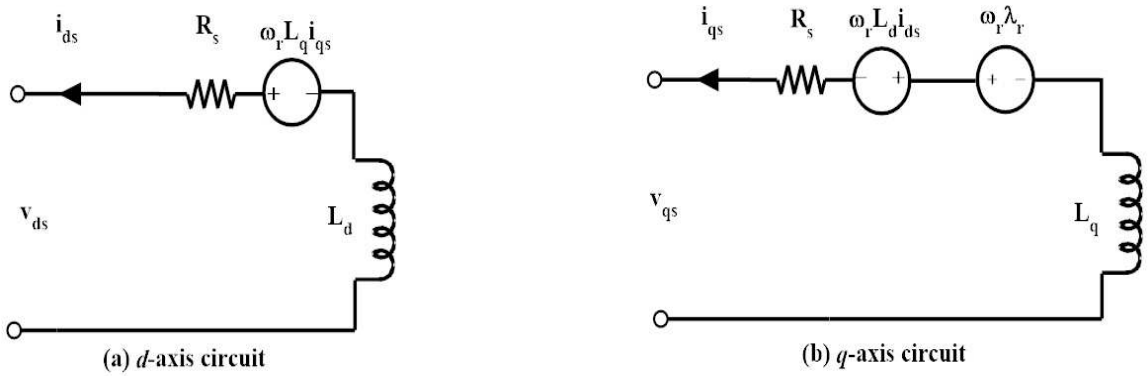


Figure 3.5: Simplified *dq*-axis Model of PMSG in Rotor-field Synchronous Reference Frame.

The stator voltage equations for the above system of PMSG can be calculated by

$$v_{ds} = -R_s i_{ds} + \omega_r L_q i_{qs} - L_d \frac{di_{ds}}{dt} \tag{3.5a}$$

$$v_{qs} = -R_s i_{qs} - \omega_r L_d i_{ds} + \omega_r \lambda_r - L_q \frac{di_{qs}}{dt} \tag{3.5b}$$

The electromagnetic torque developed by the PMSG is given by

$$T_e = \frac{3P}{2}(\lambda_r i_{qs} - (L_d - L_q) i_{ds} i_{qs}) \tag{3.6}$$

The rotor speed $\omega$ is given by equation (2.9).

To implement the dynamic model of the PMSG and study the dynamic simulation, equation (3.5) can be written as

$$\begin{aligned} i_{ds} &= \frac{1}{S}(-v_{ds} - R_s i_{ds} + \omega_r L_q i_{qs}) / L_d \\ i_{qs} &= \frac{1}{S}(-v_{qs} - R_s i_{qs} - \omega_r L_d i_{ds} + \omega_r \lambda_r) / L_q \end{aligned} \tag{3.7}$$

From the above equations, the block diagram of the PMSG can be developed and the dynamic behavior can be studied. The mechanical torque, $T_m$, the rotor flux linkage, $\lambda_r$, and the $dq$-axis stator voltages $v_{ds}$ and $v_{qs}$ are the input variables and the electromagnetic torque, $T_e$, the rotor mechanical speed, $\omega$, and the $dq$-axis stator currents $i_{ds}$ and $i_{qs}$ are the outputs.

The magnitude of stator current and voltage can be calculated using the following equations.

$$i_s = \sqrt{i_d^2 + i_q^2} \tag{3.8}$$

$$V_s = \sqrt{V_d^2 + V_q^2} \tag{3.9}$$

The active electrical power generated is calculated using the equation:

$$P_{active} = T_e \times \frac{\omega_r}{P} - 3 i_s^2 R_s \tag{3.10}$$

The total electrical power generated is calculated using the equation:

$$P_{Total} = \eta_{gen} V_s i_s \tag{3.11}$$

# CHAPTER FOUR

# COMPUTER SIMULATION OF TUBINE AND GENERATOR

The Savonius rotor and the PMSG are the main subsystems of the wind turbine system. These two subsystems can further be broken down into smaller subsystems. The flow diagram for the Simulink model is shown in Figure 4.1. These include the rotor dynamics, drive train model, stator current model, *dq* to *abc* model, voltage drop across load model, *abc* to *dq* model, and magnitude of stator current and voltage calculation. A complete model of the Savonius wind turbine system is shown in Figure 4.2.

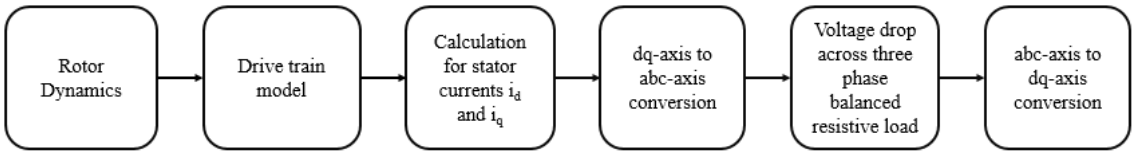


Figure 4.1: Flow Diagram for Simulink Model of PMSG.

## Rotor Dynamics

The input to the Savonius rotor is the wind speed and the angle of attack for the calculation of torque acting on the rotor. The rotor dynamics model can be seen in Figure 4.3. The rotor shaft is directly coupled with the generator shaft hence, the generator speed is equal to the wind turbine rotor speed.

## Drive Train Model

The input to the drive train model is the mechanical torque $T_m$, which is equal to the aerodynamic torque produced by the turbine blades as there is no gearbox in the system. The generator employed here is a non-salient pole permanent magnet synchronous generator. The drive train model is shown in Figure 4.4.

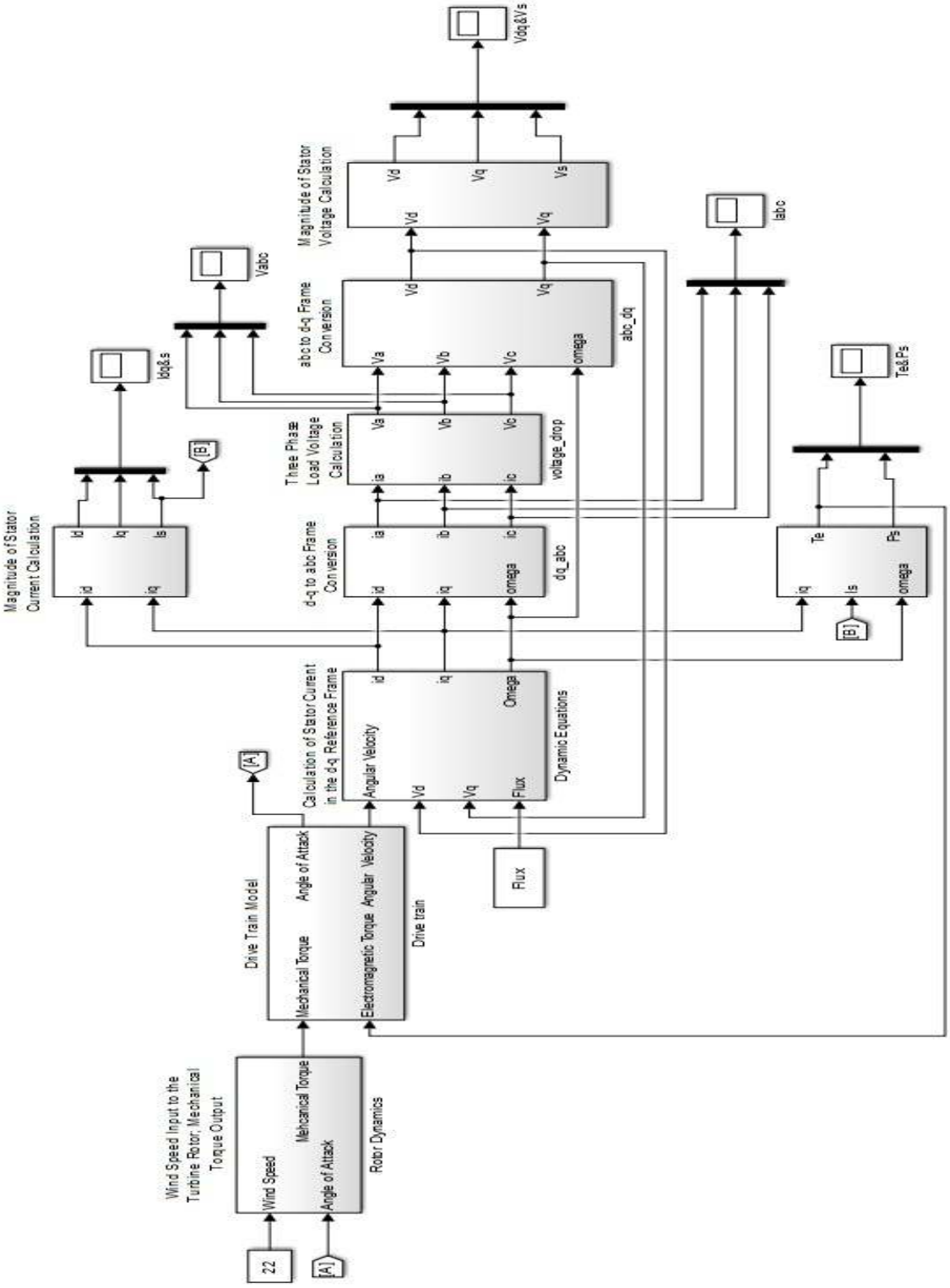


Figure 4.2: Simulink Model for Savonius Wind Turbine.

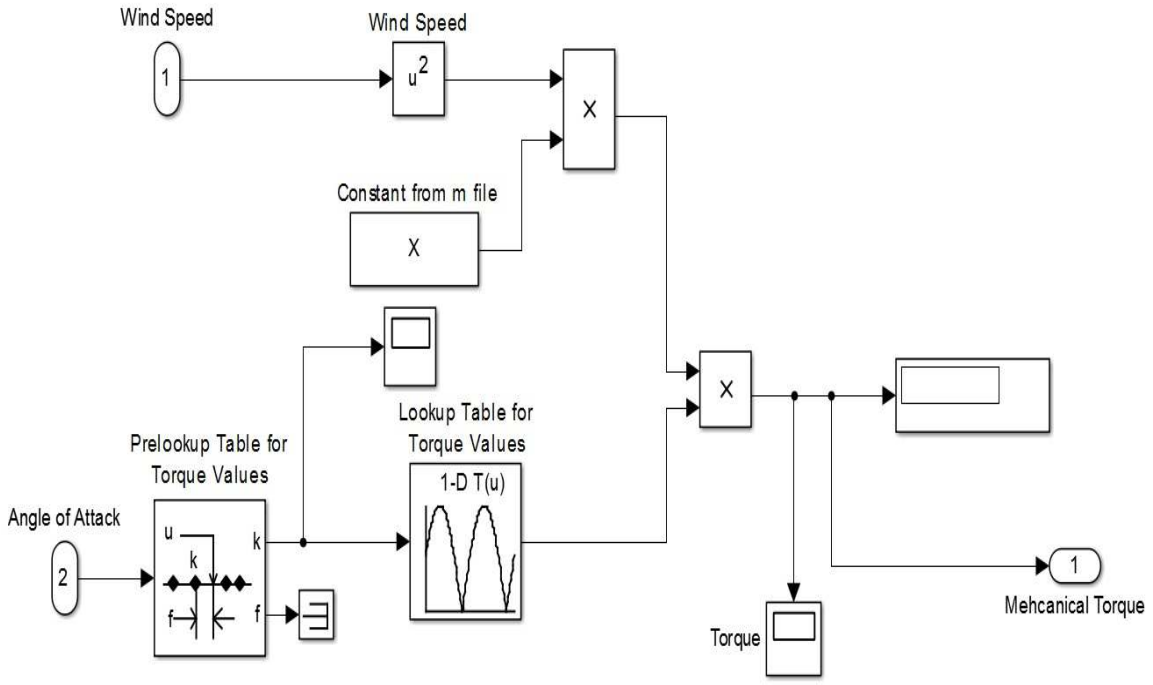


Figure 4.3: Rotor Dynamics of the Savonius Rotor.

## Stator Current Model

The output of the drive train model i.e. $\omega_e$, acts as an input to calculate the *d* and *q* components of the stator current using the equation (3.8). The load current and load voltages are supplied by a three-phase balanced load connected to the PMSG (Figure 4.5).

## *dq* to *abc* conversion model

The *d-q* components of the load current are converted to the *abc* (three-phase) components using the reference frame theory. The conversion of the components is done according to the equation (3.3) and is shown in Figure 4.6.

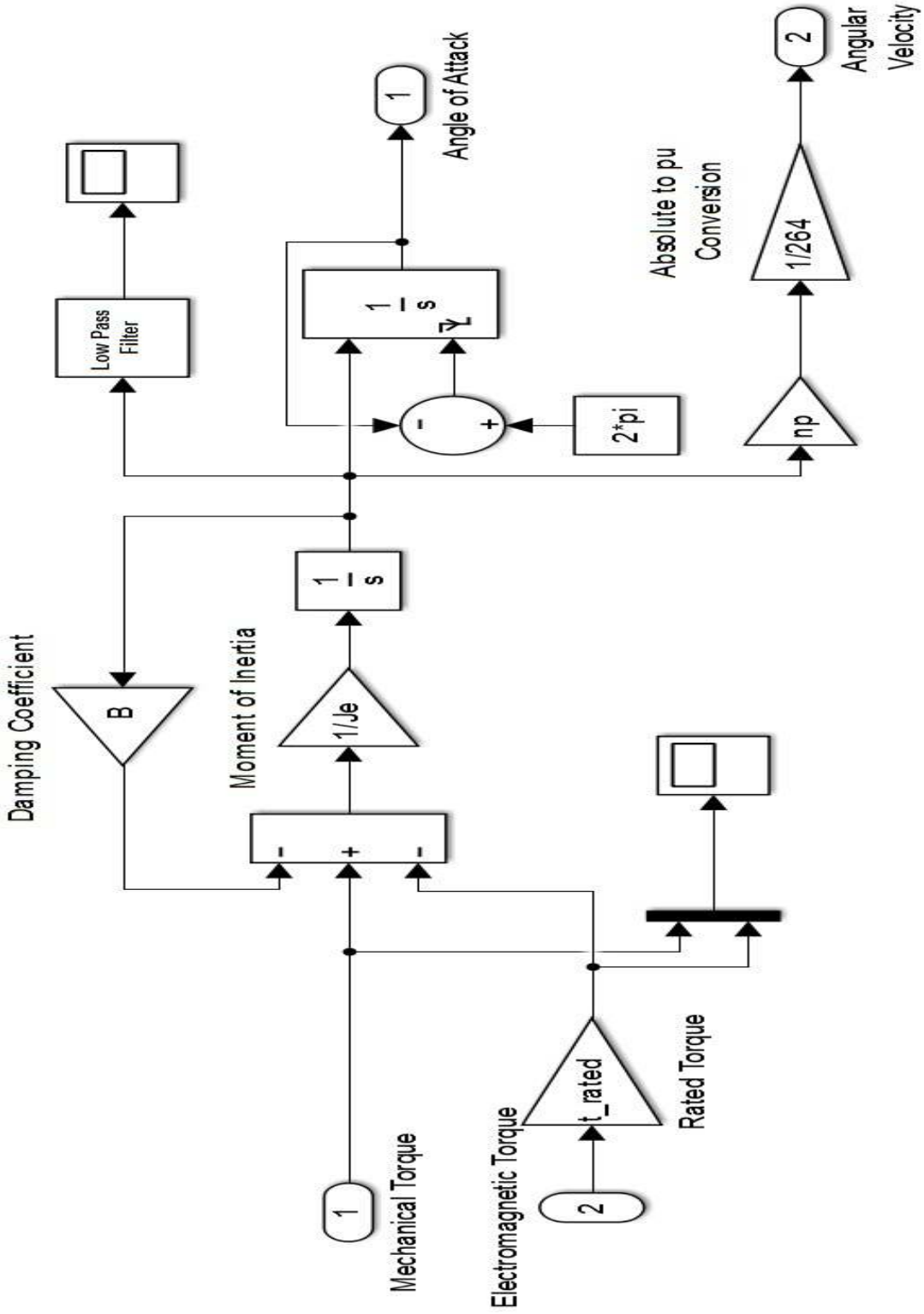


Figure 4.4: Drive Train Model.

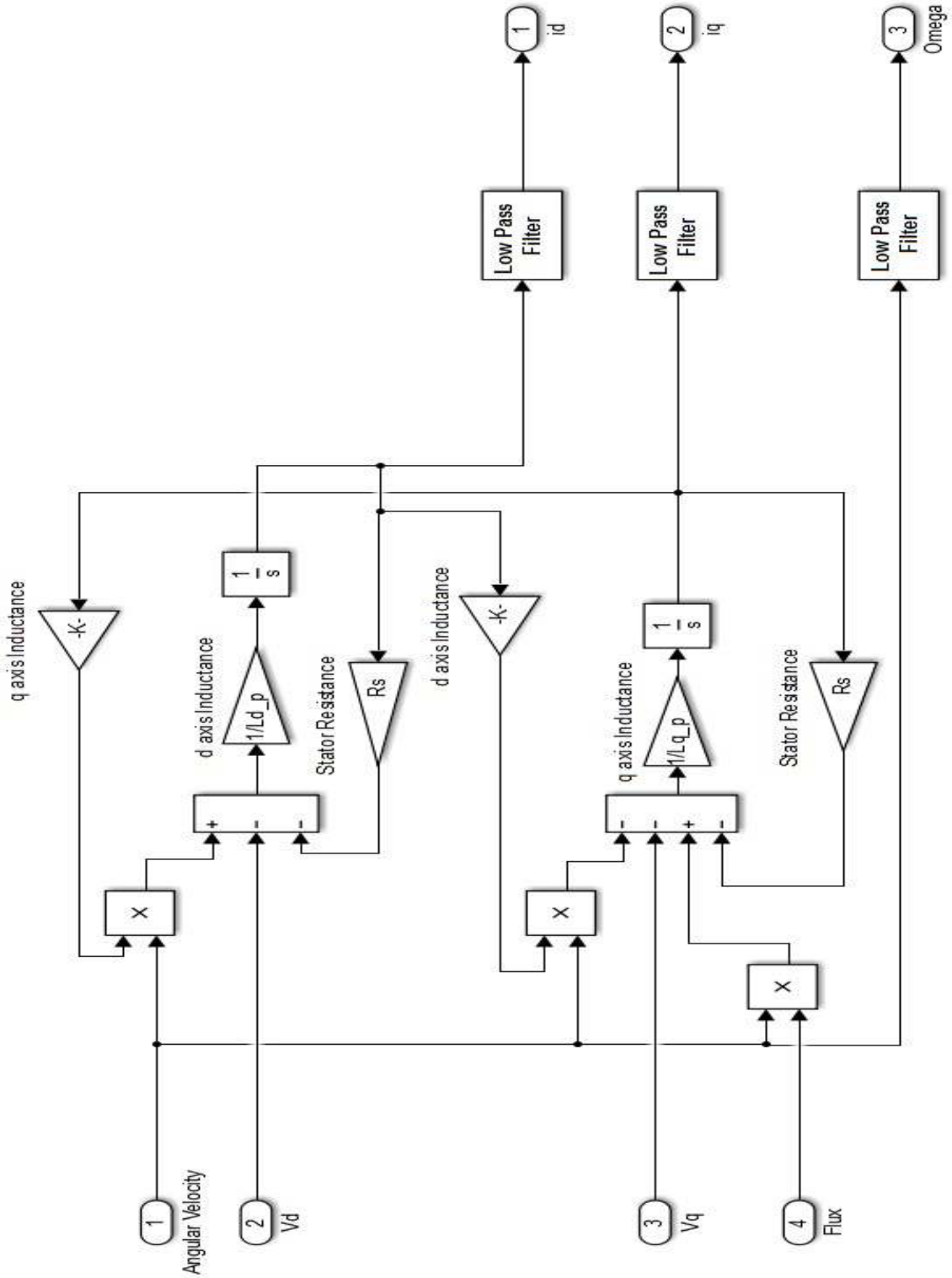


Figure 4.5: Stator Current ($i_{dq}$) Model.

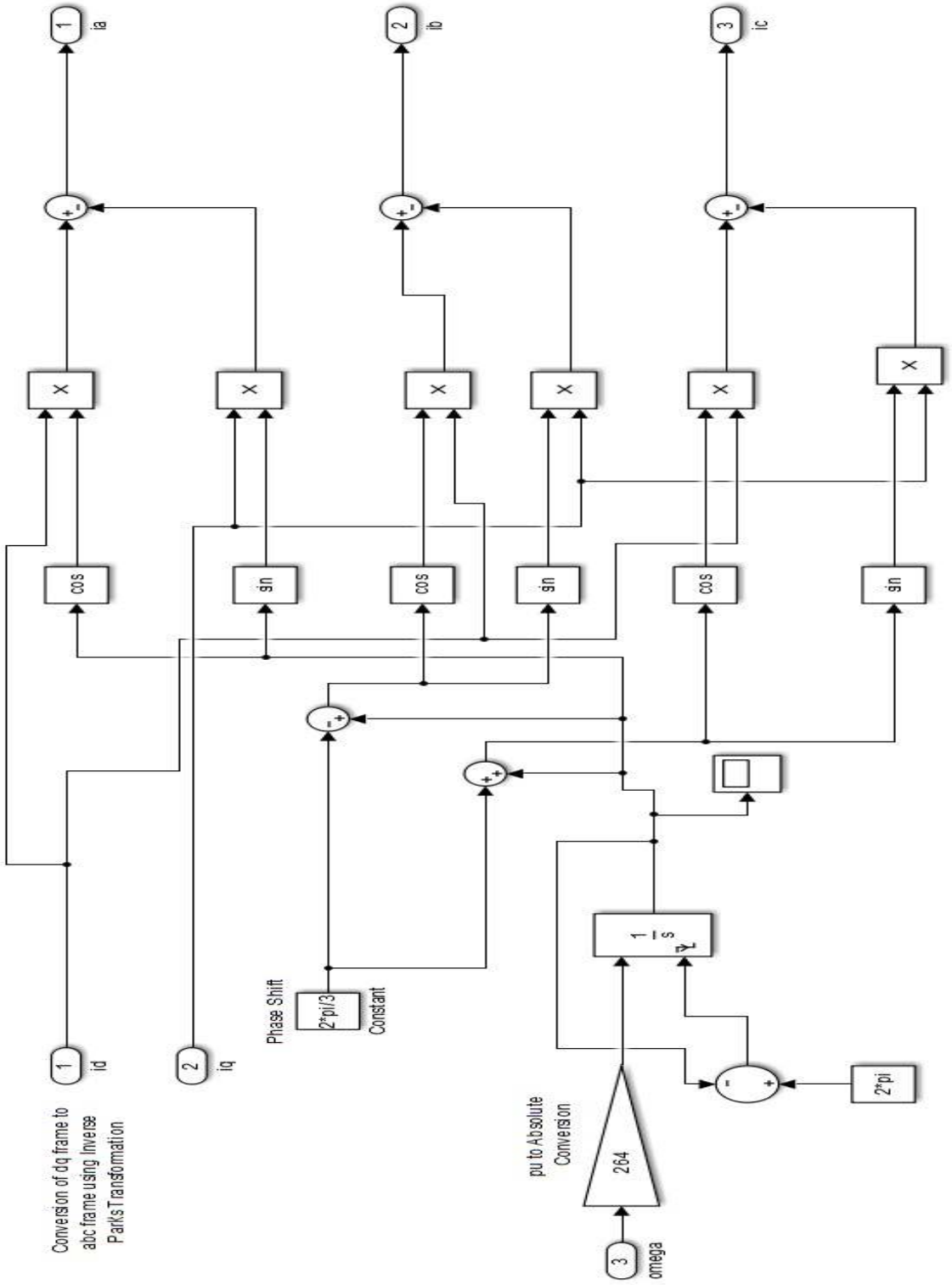


Figure 4.6: *dq* to *abc* Conversion Model.

Load Voltages and *abc* to *dq* Conversion Model

The load voltages across the three-phase balanced resistive load are calculated using the Ohm's law. The Simulink model of the subsystem is as follows:

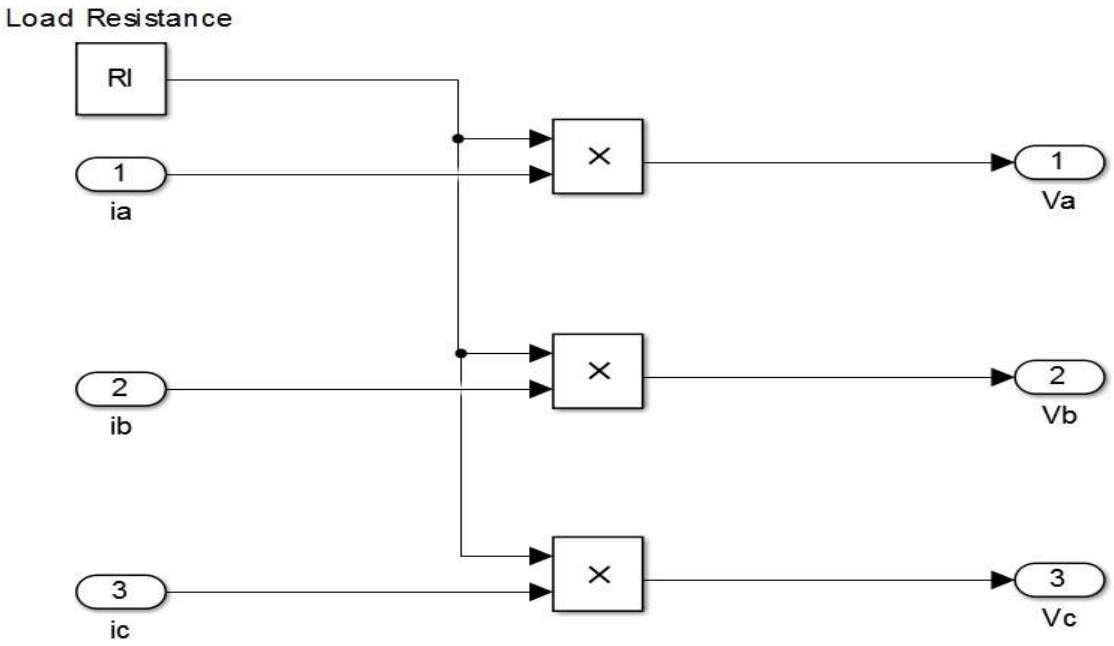


Figure 4.7: Voltage Drop Across Electrical Load Model.

The *d*- and *q*-components of the voltage drop across the resistance is the input to the stator current model. So, an *abc* to *dq* conversion (Figure 4.8) is required and then the output are fed to the stator current model. The *abc* to *dq* conversion is done using the equation (3.1).

The electromagnetic torque and the electrical power (Figure 4.9) generated are calculated using the equations (3.6) and (3.11), respectively. Also, the magnitude of the stator current (Figure 4.10) and voltage (Figure 4.11) is calculated using equations (3.8) and (3.9), respectively.

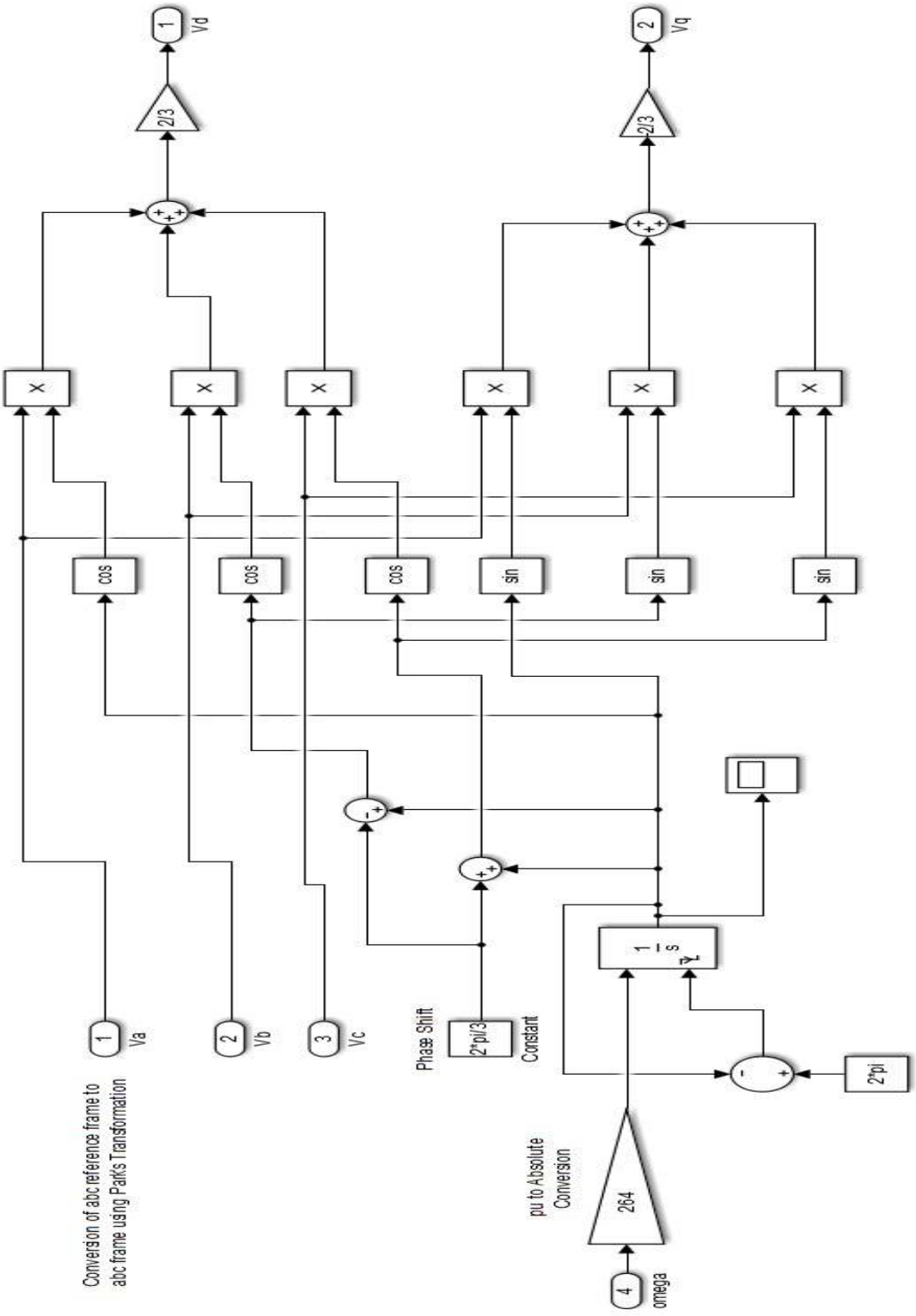


Figure 4.8: *abc* to *dq* Conversion Model.

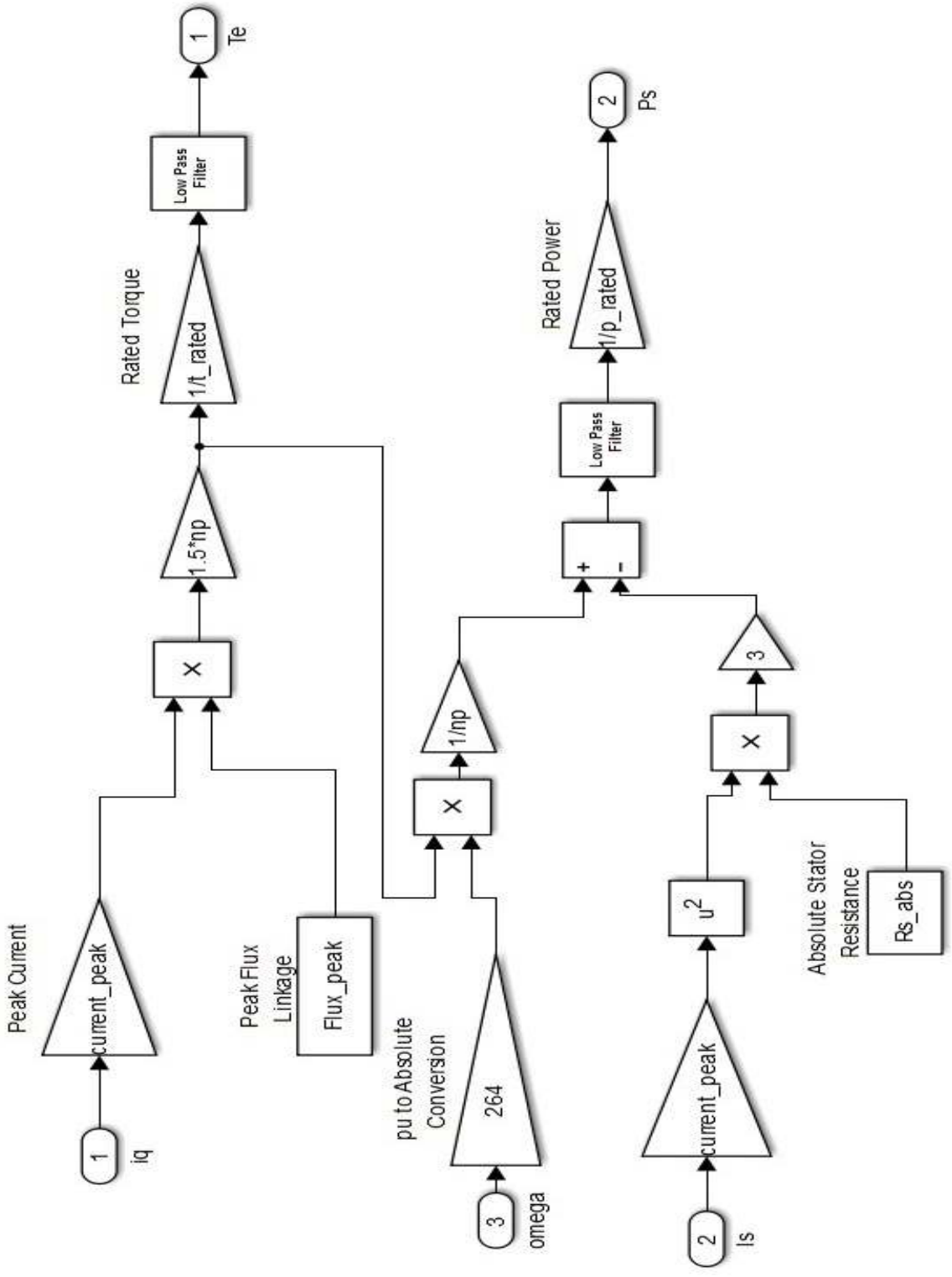


Figure 4.9: Electromagnetic Torque and Electrical Power Model.

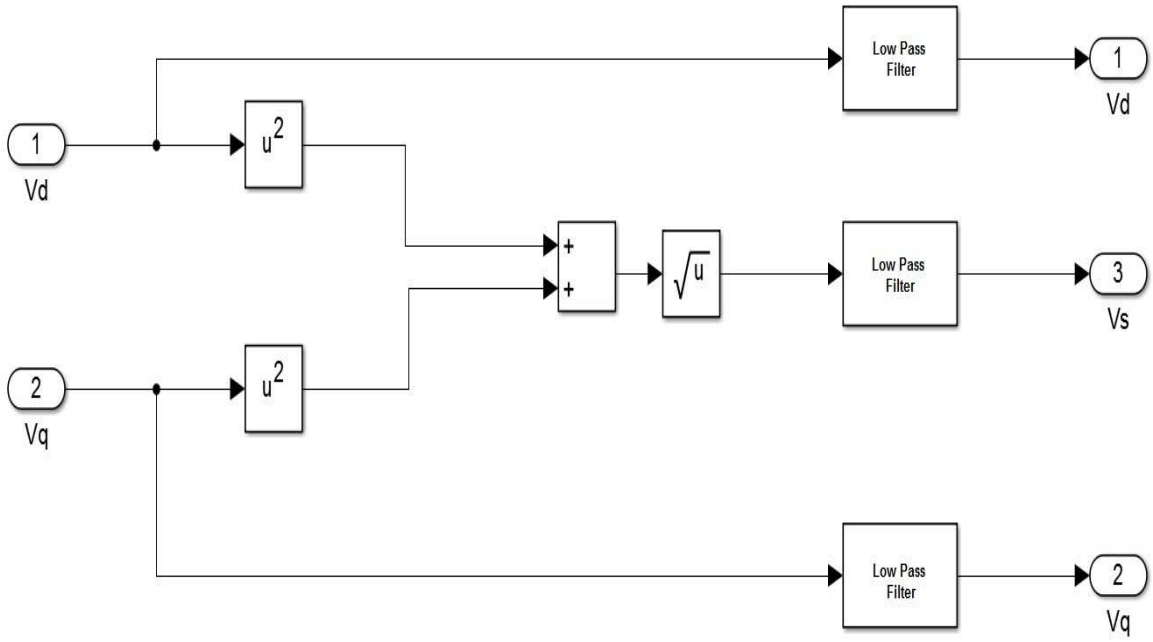


Figure 4.10: Stator Voltage Magnitude Model.

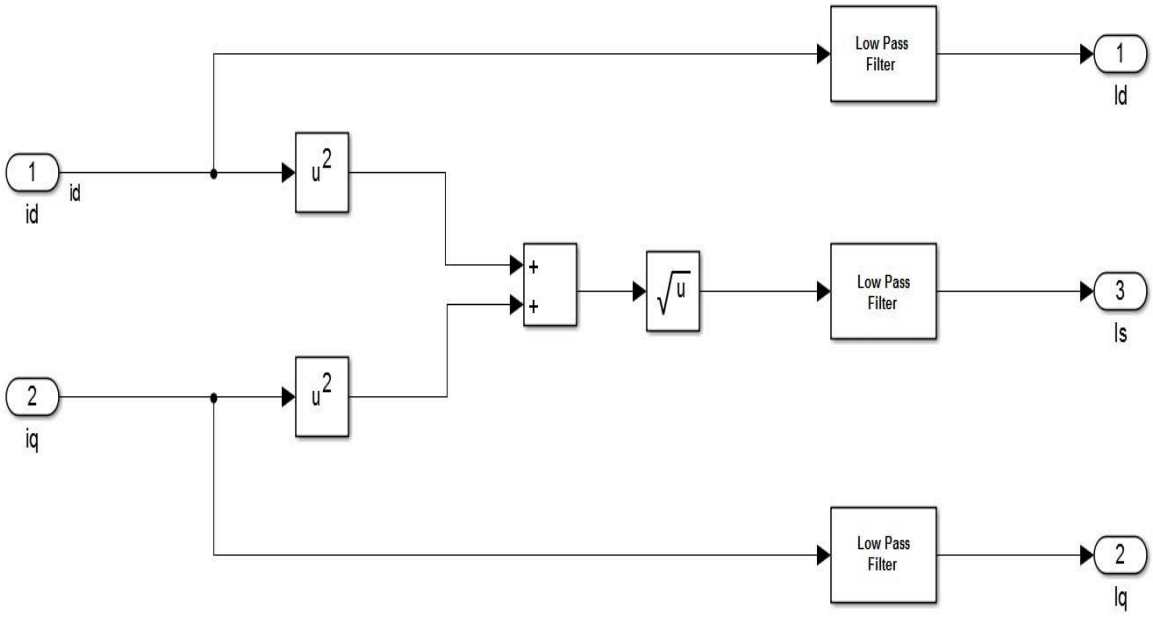


Figure 4.11: Stator Current Magnitude Model.

# CHAPTER FIVE

# EXPERIMENTAL WIND TURBINE SYSTEM

The Savonius wind turbine that is used for obtaining the experimental results is shown in Figure 5.1. The rotor is made of stainless steel sheets that are rolled to form the buckets that are rigidly mounted on the wooden end plates. The rotor shaft connects the rotor to the generator located at the base of the rotor. The entire system is enclosed within a solid aluminum frame to provide stability, also, the frame is enclosed within a wire net to prevent any injury while operation. The wind turbine is driven by a blower placed in front of the turbine.

Figure 5.1: Experimental Savonius Wind Turbine.

An anemometer is provided with the system to measure the wind speed. The wind speed is measured with the help of a NPN type proximity switch (Figure 5.2) by Square D (Class 9006 Type PJA112N Series A) and a small magnet that is fixed to the anemometer hub. Another proximity switch (Figure 5.2) by Square D (Class 9006 Type PJD112N Series A) is used to measure the rpm of the wind turbine. The sensor is attached at the base of the frame and a magnet is placed at the bottom of the end plate.

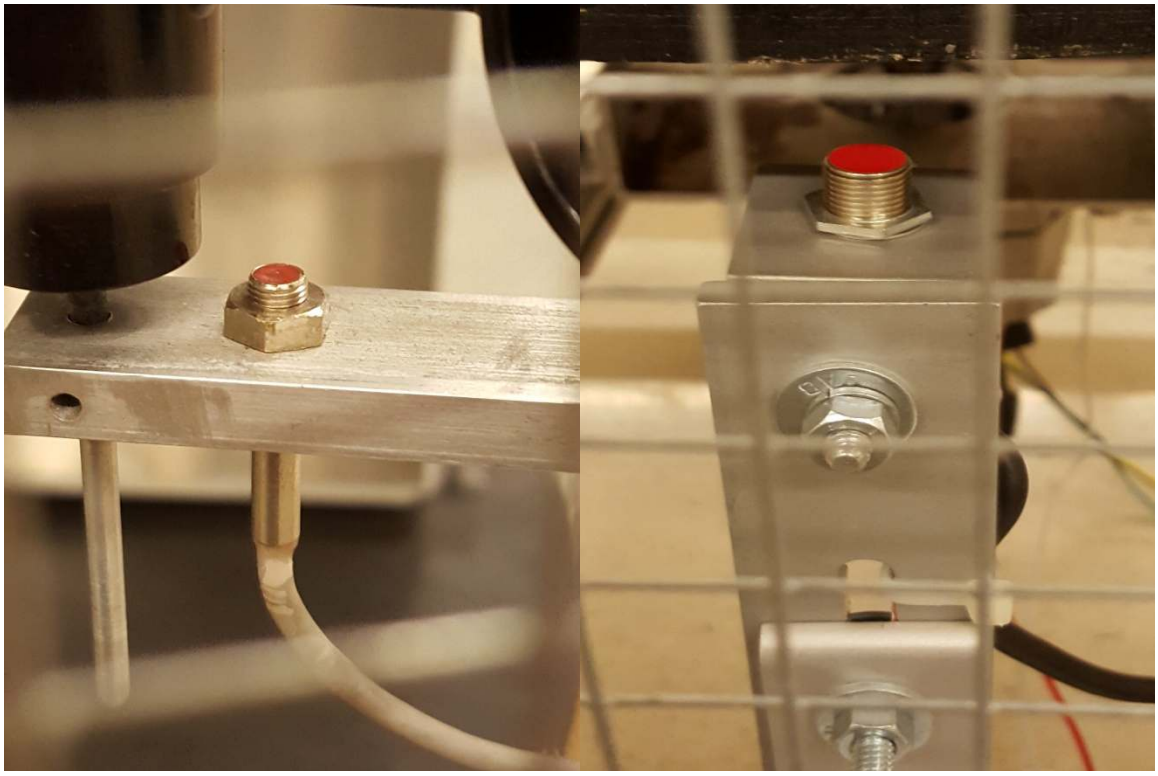

Figure 5.2: Proximity Sensors Used for RPM Measurement.

The frequencies generated by the wind speed sensor and turbine rotor sensor are converted to DC voltage using Frequency to Analog converters (Figure 5.3). The FACs are calibrated to produce an output of 0-10 VDC in proportion to the input frequency.

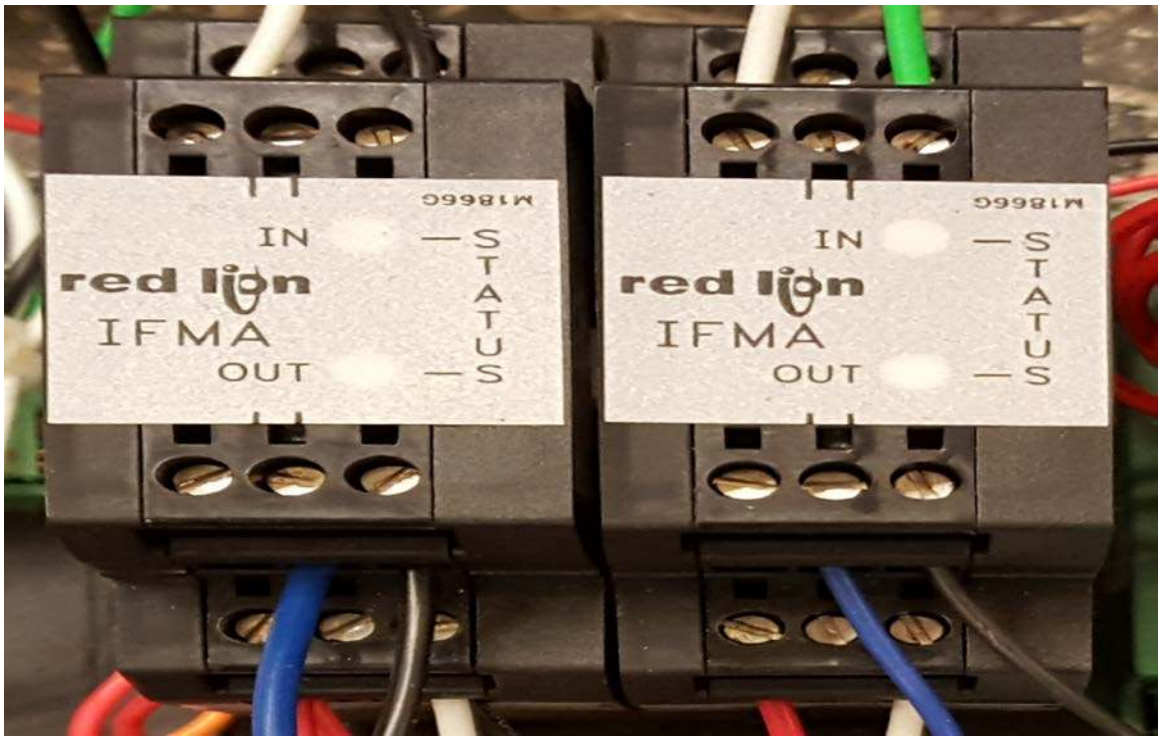


Figure 5.3: Frequency to Analog Converters.

Table 5.1: List of Material Used for Turbine Fabrication.

| **Materials** | **Dimensions** | |
|---|---|---|
| Aluminum sheet | Thickness=0.0076 m | Length=1.12 m, Width=0.58 m |
| Bearings | Quantity=2 | |
| Extruded aluminum frame | Length=13.10 m | Height=0.0254 m |
| Shaft | Length=1.20 m | Diameter=0.0254 m |
| Stainless steel net | Length=1.092 m | Height=1.175 m |
| Wooden sheet | Thickness=0.0127 m | Diameter=0.82 m |

A permanent magnet alternator is used as the generator in the system (Figure 5.4). The Wind Blue DC-540 (Wind blue power, June 2015) is a low wind generator which is used in areas that experience low wind speeds. The 3-phase AC voltage output of the generator is converted to DC voltage using a rectifier and charge controller (Figure 5.5). The charge controller is used to prevent any overload on the system by braking the voltage at 15 V.

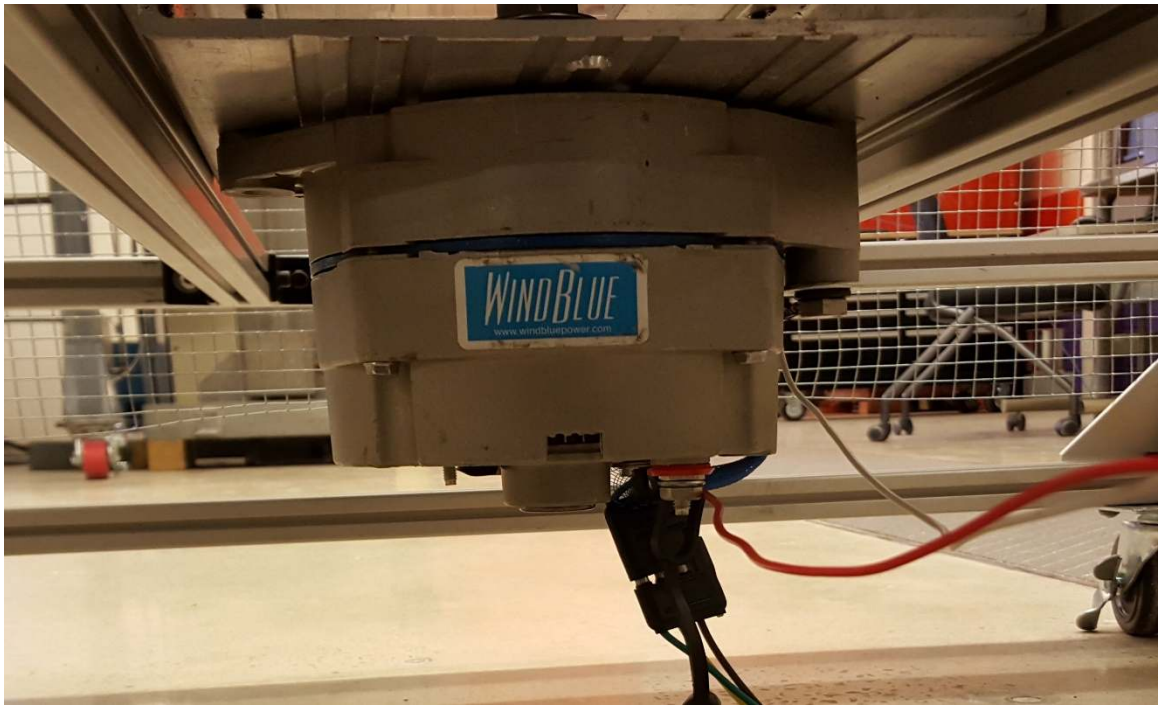


Figure 5.4: Permanent Magnet Alternator.

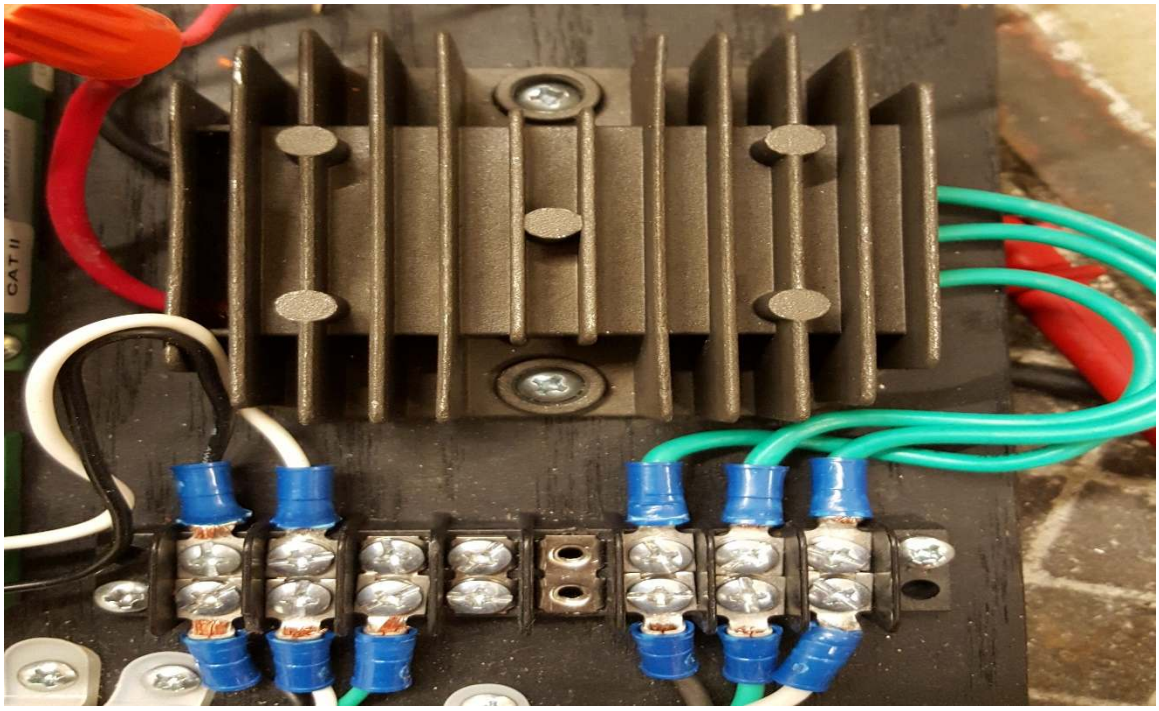


Figure 5.5: Rectifier and Charge Controller.

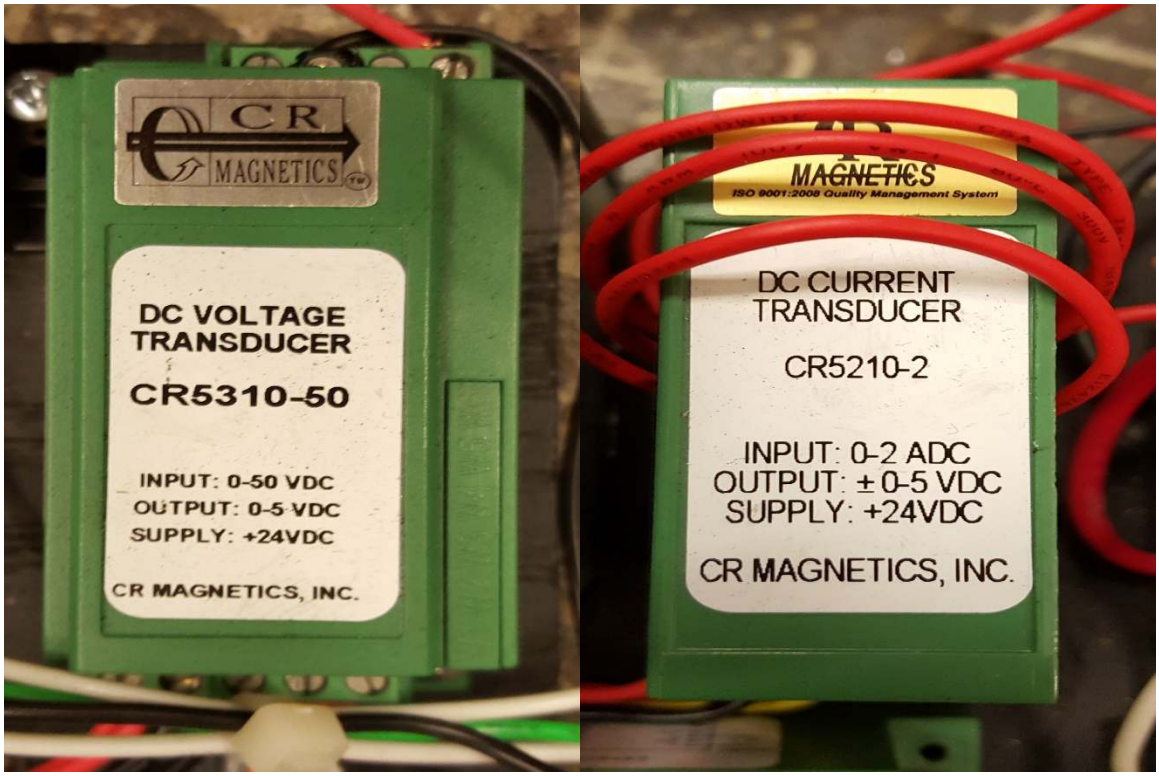


Figure 5.6: Voltage and Current Transducers.

The voltage and current in the system are measured across a load using a DC voltage transducer and DC current transducer respectively shown in Figure 5.6. Two 12 VDC fans (Figure 5.7) and a LED are the load on the system. The LED is used for a visual detection of the power being produced by the system.

National Instruments USB-6001 is the data acquisition device used to acquire the signals from the sensors and the generator Figure 5.8. LabView software is used for creating a virtual instrument (VI) on a PC for acquiring data from the DAQ (Koch-Ciobotaru, 2010). A complete list of materials and components used are shown in Table 5.1 and Table 5.2. The block diagram of the experimental system below (refer to Figure 5.10) shows all the connections and devices used for data analysis and obtaining results.

Table 5.2: List of Components Used for Obtaining Results.

| **Part** | **Manufacturer** | **Part Number** | **Specs** |
|---|---|---|---|
| Alternator | Wind Blue | DC 540 | 3 phase AC |
| Blower | Triple S | Mach III | 1 HP, 4100 CFM, 110 VAC |
| Current Transducer | CR Magnetics | CR5200-2 | 0-2 ADC, 0-5 VDC, 24 VDC |
| DAQ card (ADC) | National Instruments | USB 6001 | USB powered |
| Frequency to Analog Converter (Quantity = 2) | Red Lion Controls | IFMA0035 | 1 Hz - 25 kHz, 0-10VDC, 24 VDC |
| Power Supply | CR Magnetics | CRPS24VDC-120 | 24 VDC, 110 VAC |
| Proximity Sensor 1 | Square D | Class 9006 Type PJA112N | 9-32 VDC |
| Proximity Sensor 2 | Square D | Class 9006 Type PJD112N | 9-32 VDC |
| Rectifier | Misol | WDT-FW-1203-1 | 300 W 12, 15 V Brake Voltage |
| Voltage Transducer | CR Magnetics | CR5310-50 | 0-50 VDC ,0-5 VDC, 24 VDC |

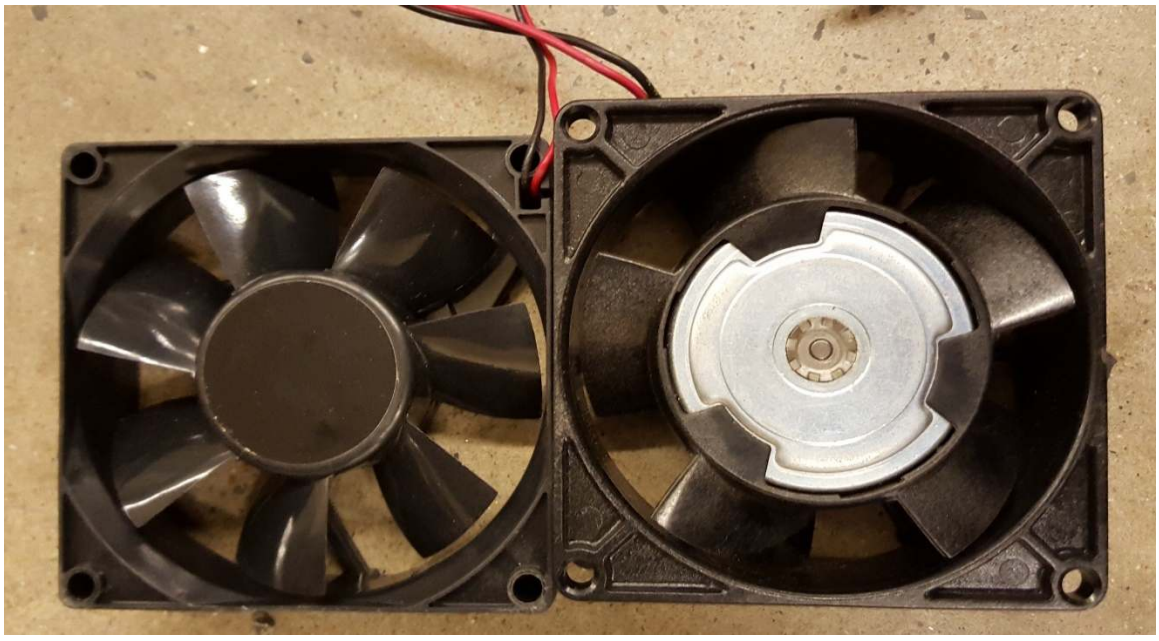

Figure 5.7: Two 12 VDC Fans Used as Electrical Load.


Figure 5.8: National Instruments Data Acquisition System.


Figure 5.9: Blower Used for Wind Turbine.

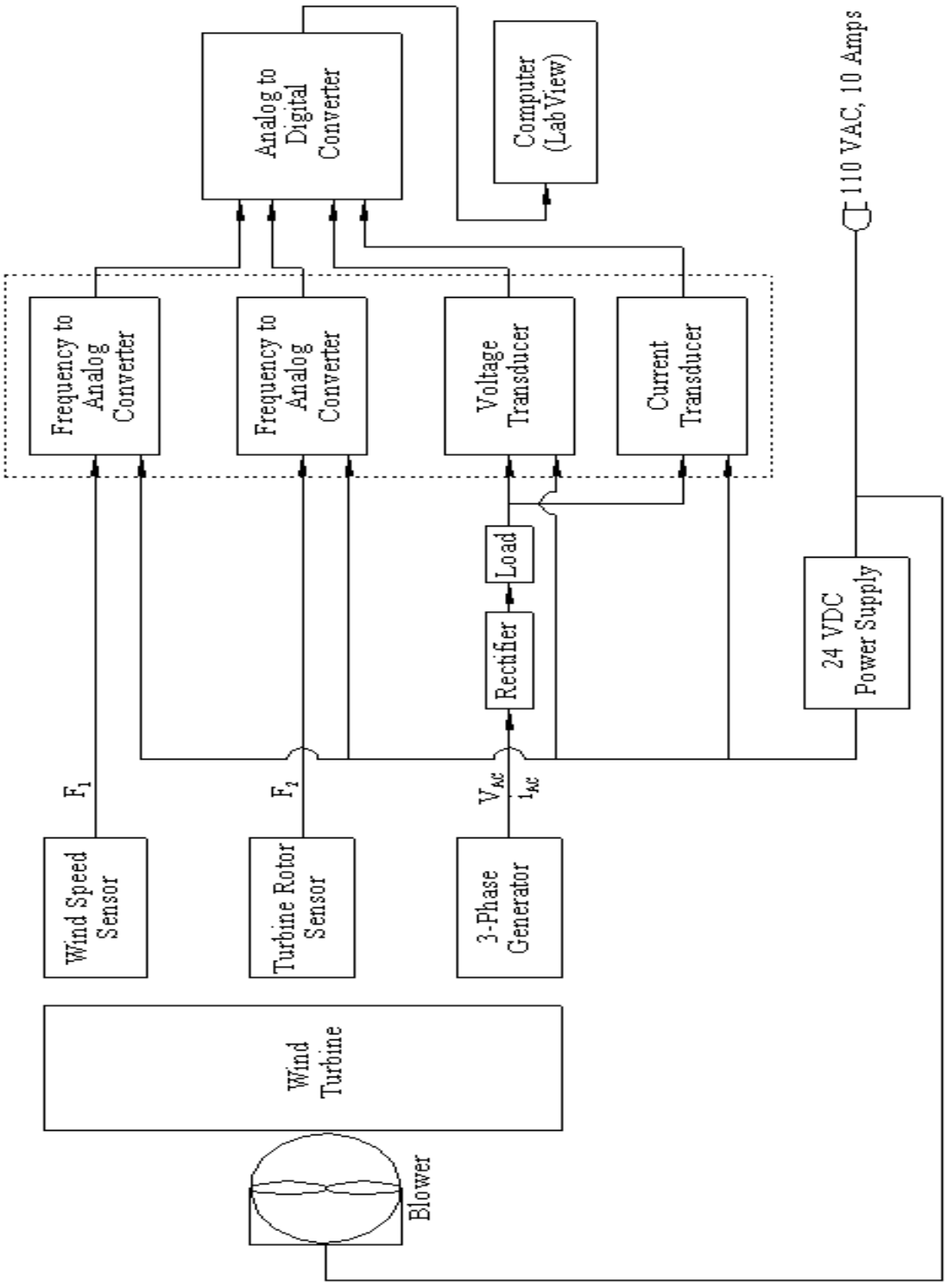


Figure 5.10: Block Diagram of the Experimental System.

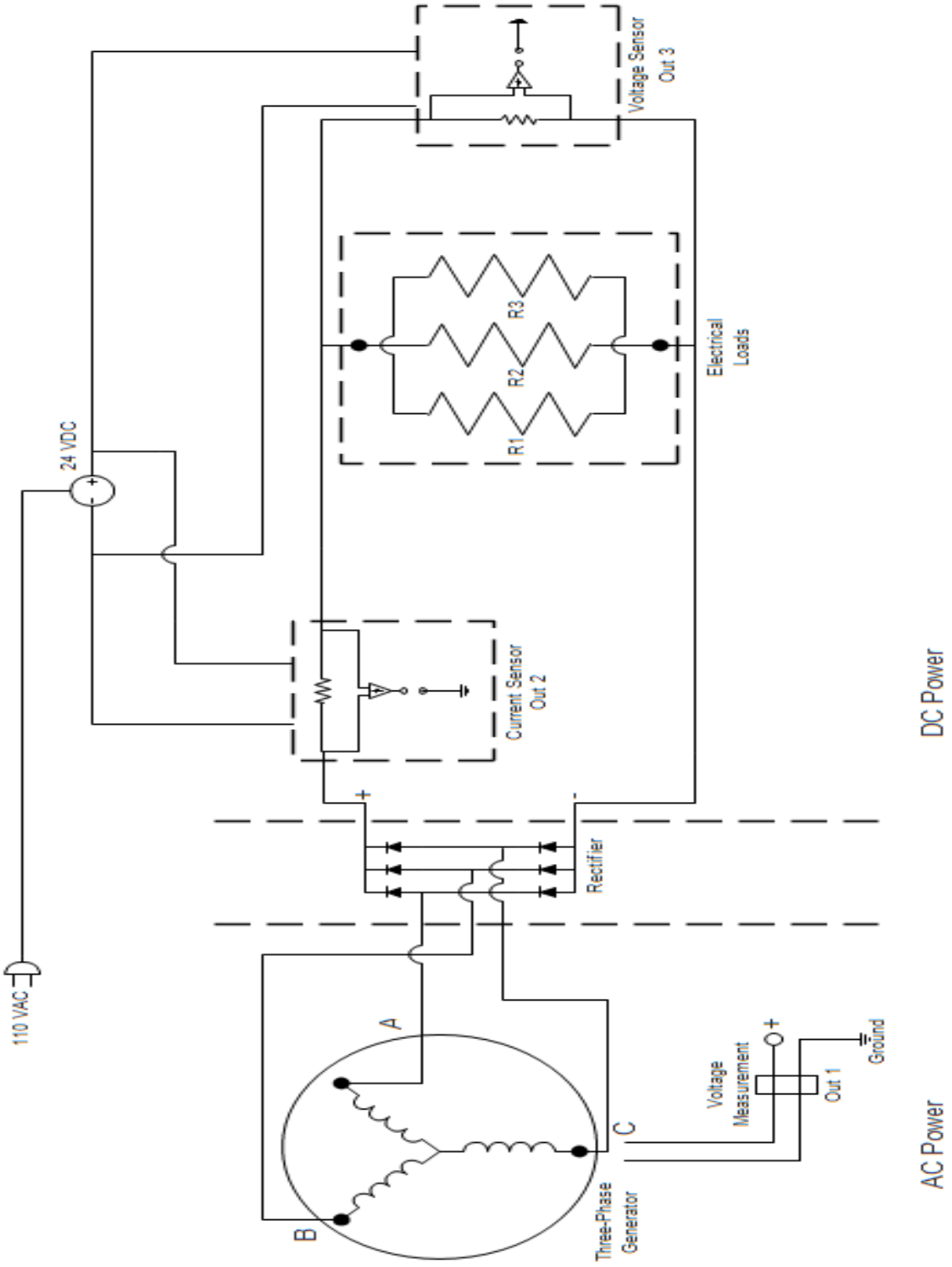


Figure 5.11: Electrical Schematic Diagram of the System.

# CHAPTER SIX

## DISCUSSION OF EXPERIMENTAL AND NUMERICAL RESULTS

This chapter contains all the results acquired from the experimental setup and the simulation. NI data acquisition device has been used to extract the data from the various sensors and transducers in LabView software. The simulation has been performed in MATLAB/Simulink environment.

The experimental and numerical results have been acquired to make a comparison between the two results. The experimental results have been acquired at three different wind speeds (16.9 m/sec, 19.8 m/sec, and 21.9 m/sec), corresponding to the three levels on the blower. The outputs have been recorded using an electrical load of two 12 VDC fans. The mathematical model was developed in MATLAB/Simulink using the equations per Appendix B. The numerical results have been acquired using the parameters from the Experimental Savonius rotor (Table D.3) and 1 kW Permanent Magnet Synchronous Generator as per Table D.3. From the testing performed in this study, the proposed mechanical efficiency is 70% considering the weight and instability of the experimental system, and the generator has an efficiency of 33% from the data provided by the manufacturer.

In Figures 6.1a and 6.1b, the experimental results for the voltage and current are plotted against the wind speed corresponding to the three blower speed levels, respectively. Figure 6.1 shows the feasibility of generating measurable power from the experimental system. It can be concluded that power generated is low but, it provides a starting point for further investigation.

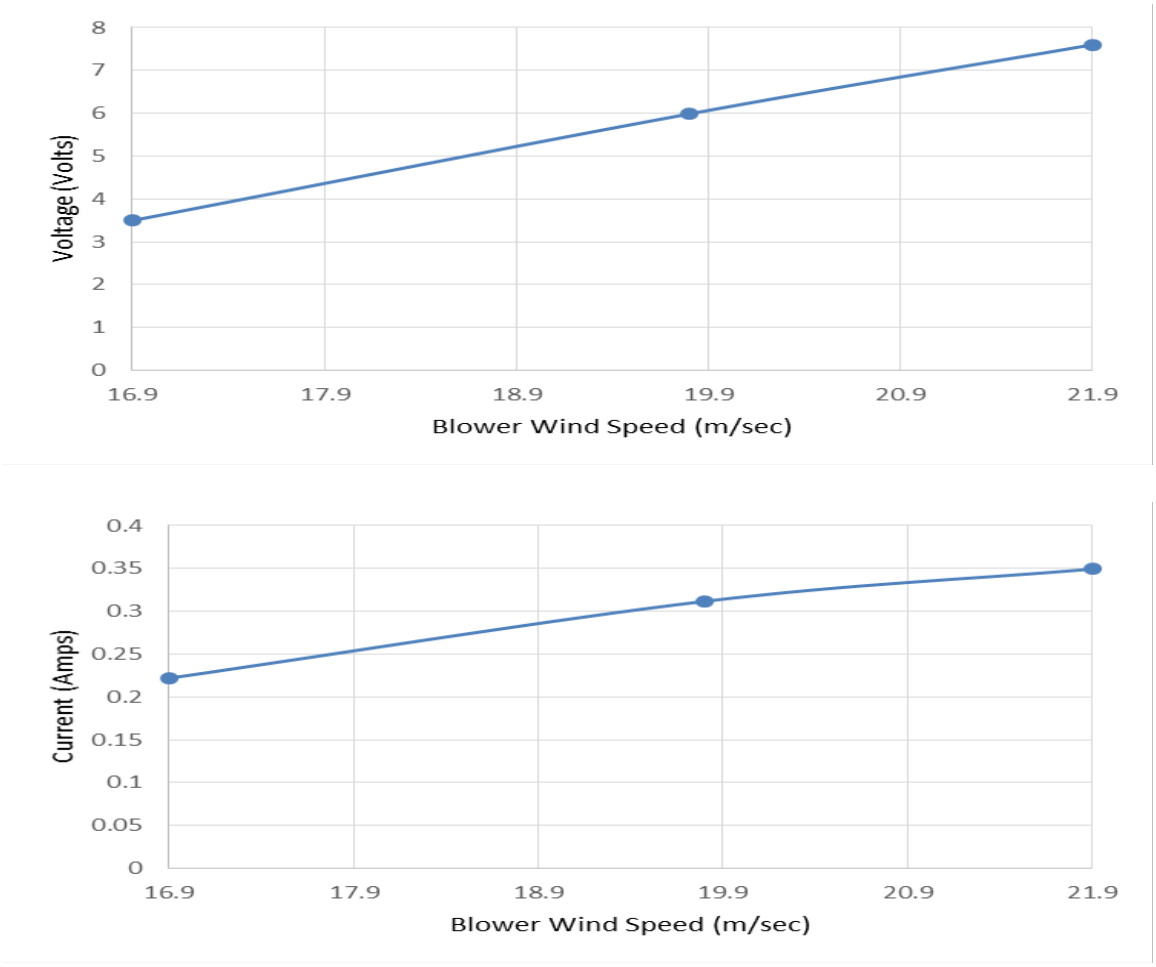


Figure 6.1: Experimental Results versus Blower Level: a) Voltage, and b) Current.

Figures 6.2a, 6.2b, and 6.2c shows the dynamic data for the voltage, current, and power generated by the experimental system at different blower levels and wind speeds, respectively. The experimental system has been run for a total of 30 minutes, 10 minutes at each blower setting/ wind speed. It can be observed that the system stabilizes in a short time and the power output has a maximum value of 2.7 Watts at a wind speed of 21.9 m/sec. The signals also have some chattering which is due to the environmental factors. Looking at the data sheet provided by the manufacturer of Wind Blue DC-540, we should be generating 4.5 W but, we are only producing 2.7 W electrical power. In order to generate

the desired power, the rpm needs to be increased from 115 to 500 rpm by using a gear train in the system.

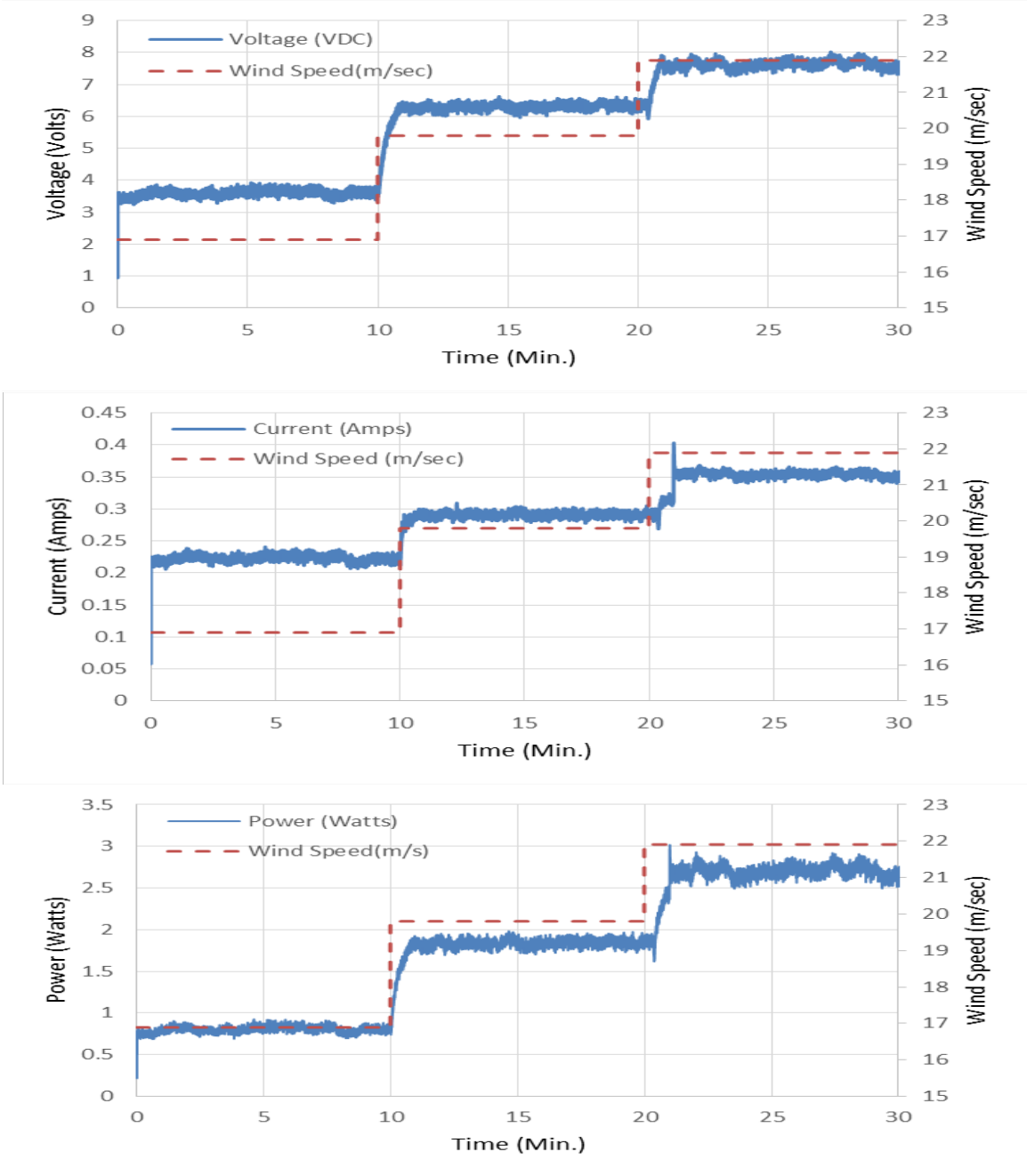


Figure 6.2: Experimental Results with measured: a) Voltage, b) Current, and c) Power versus time for three wind speeds.

The numerical results from the MATLAB/Simulink simulation are shown below. The numerical results are obtained at a wind speed of 21.9 m/sec. Figures 6.3a and 6.3b show the three-phase electrical voltage and current produced by the PMSG. The three-phase electrical voltage and current reach a steady state value around 10 sec but the response has been plotted for only 2 sec to provide a clearer look at the oscillations of the outputs. The voltage and current values are in pu (per-unit) and plotted versus time. The comparison of the following results with the paper by El-Saady *et al*., 2013, show similar result profiles but the magnitudes differ due to different generator parameters.

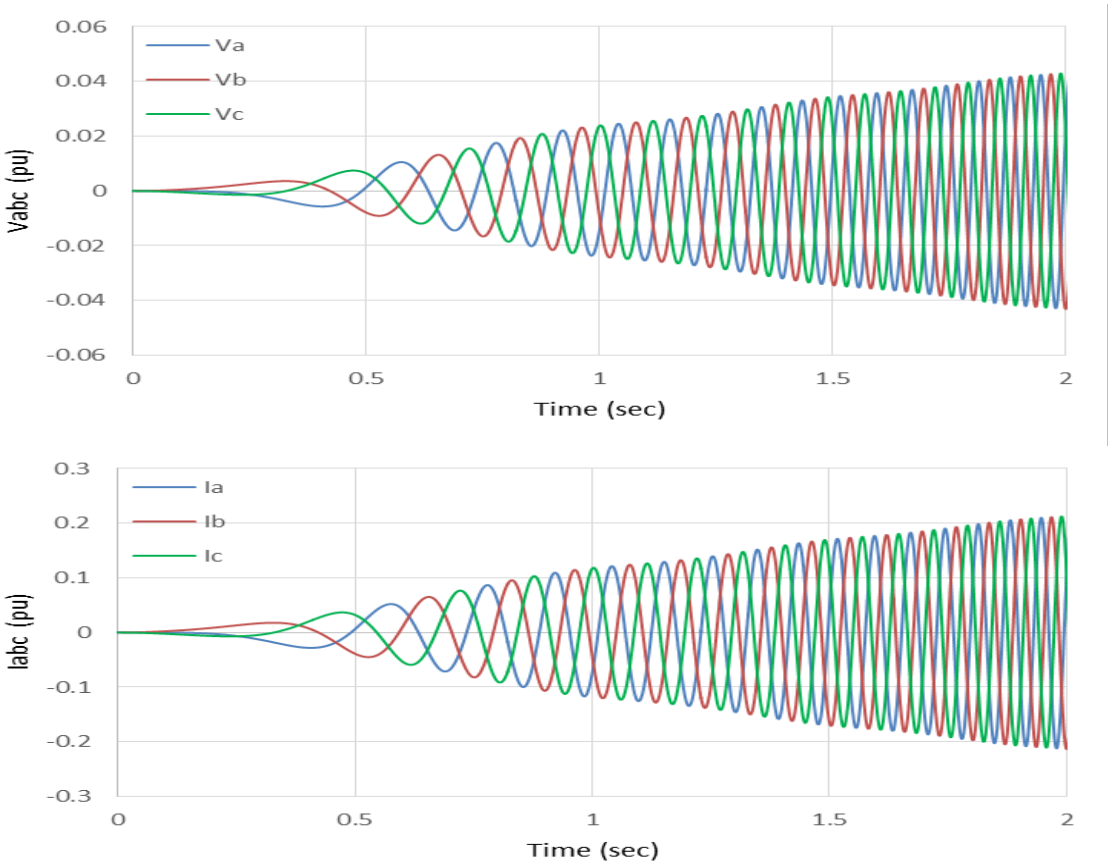


Figure 6.3: Simulation Results for the Permanent Magnet Electric Generator - a) Three-phase Voltage; and b) Three-phase Current.

The direct and quadrature components of the voltage and current are shown in Figures 6.4a and 6.4b, respectively. The magnitude of the voltage produced is also shown, denoted by Vs (6.4a) and the magnitude of current is denoted by Is (6.4b). It can be observed that after t = 20 sec, the *d*-axis components of voltage and current become zero and therefore the magnitude becomes equal to the *q*-axis component. The outputs values are in pu (per-unit) system and are converted to absolute values later for comparison. Similar validation process has been followed for the direct (*d*-axis) and quadrature (*q*-axis) components of the voltage and current as for the three-phase electrical voltage and current.

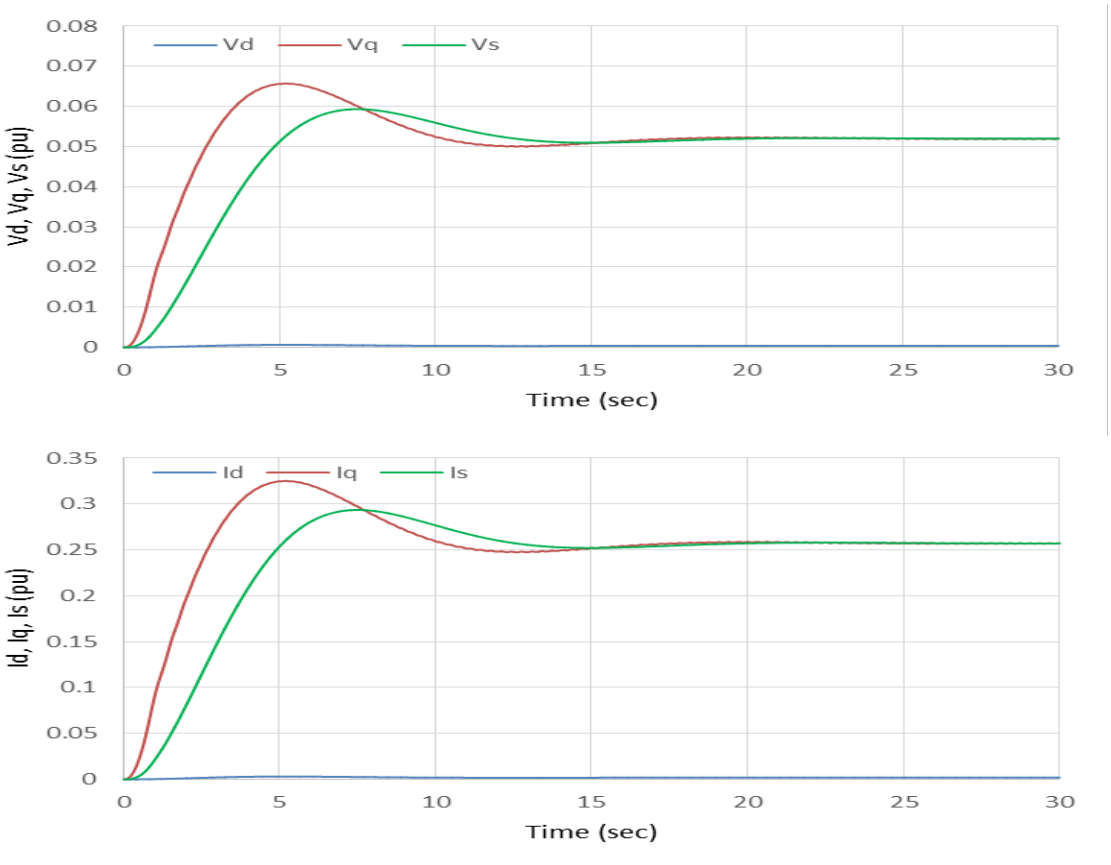


Figure 6.4: Numerical Results for Generator Model - a) Direct and Quadrature Component, and Magnitude of Voltage, and b) Direct and Quadrature Component, and Magnitude of Current.

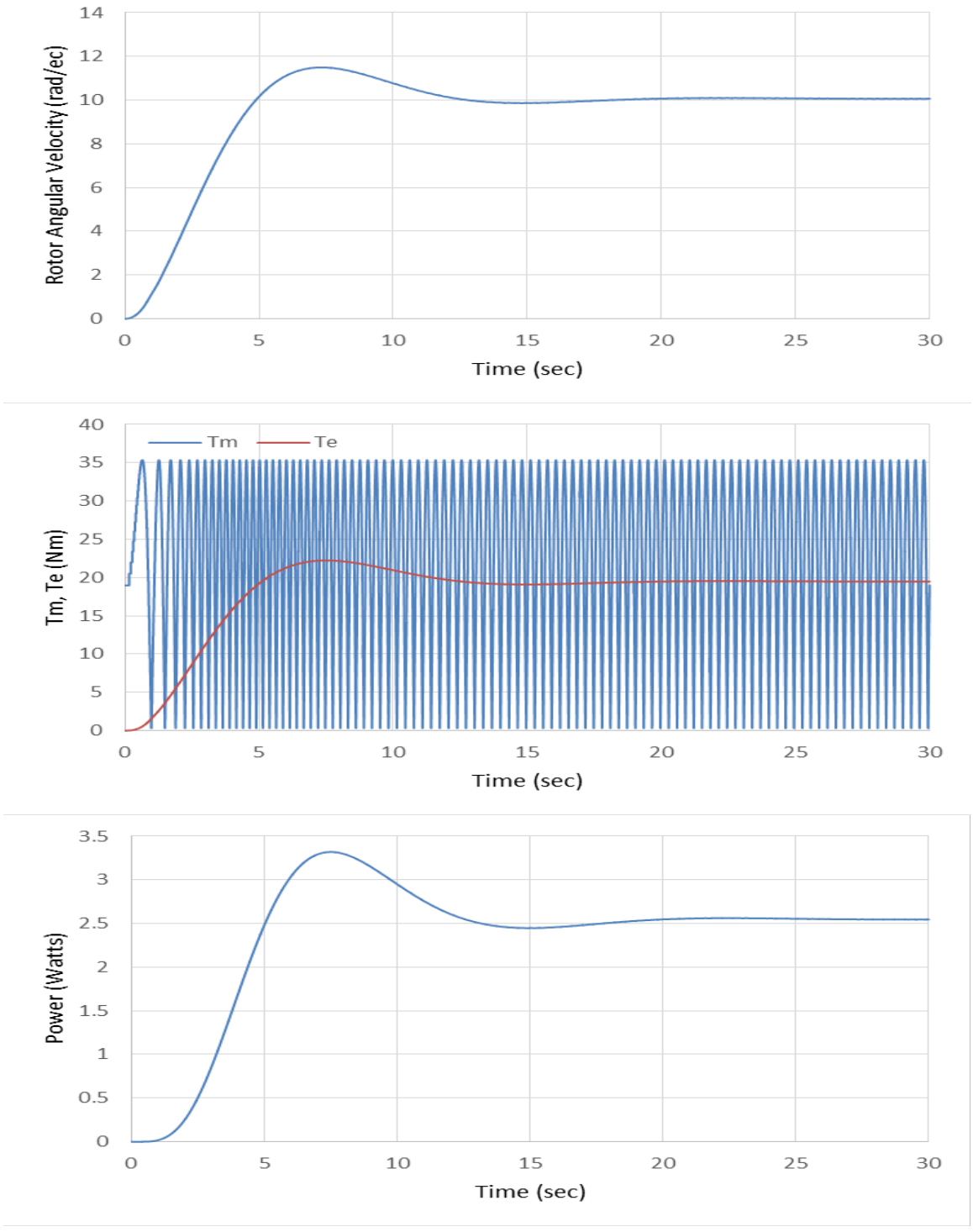


Figure 6.5: Numerical Results for the: a) Angular Velocity of the Rotor, b) Mechanical and Electromangentic Torque Generated, and c) Total Electrical Power Generated by Wind Turbine.

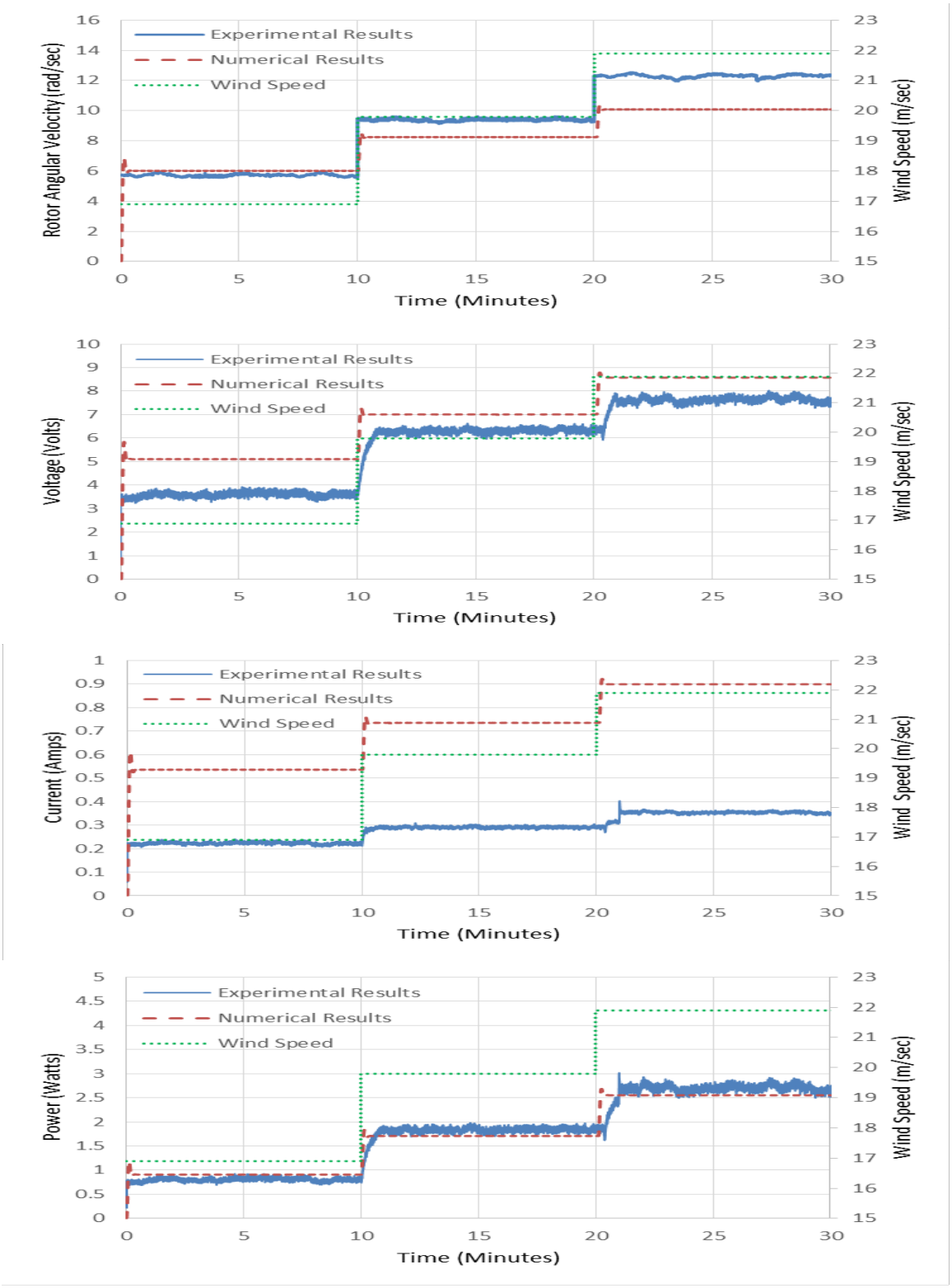


Figure 6.6: Comparison of Experimental and Numerical Results at Three Different Wind Speeds: a) Voltage, b) Current and c) Total Electrical Power Generated.

Figure 6.5a shows the angular velocity of the wind turbine rotor. From the response it is evident that it is a second order system and finally settles at a 96 rpm at t = 20 sec. Figure 6.5b shows the input mechancal torque to the generator, and the electromagnetic torque developed by the generator. Since, the mechanical torque (Equation (7)) is a function of sin and cos, the result is oscillatory and the value oscillates between 0-35 Nm. It can be observed that the generated electromagnetic torque follows the rotor angular velocity profile and settles at 20 Nm. The rotor angular velocity drives the generator and electromagnetic torque is a result of generator motion. The generator electrical power generated is depicted in Figure 6.5c. The generated electrical power is sufficient to run a LED and two 12 VDC fans connected in parallel but, we want to generate more power for battery charging and running electrical devices.

Figure 6.6 shows the comparison between the experimental and numerical results of rotor angular velocity, voltage, current, and total electrical power generated at three different wind speeds. It can be observed that there are differences in the numerical and experimental results which are caused due to limitations of the mathematical model and experimental system. For example: there is a 16%, 11%, 61% and 4% difference between the simulation and test results at a 21.9 m/sec operating wind speed. The possible explanation for the difference is discussed in the following paragraph. We want the difference to be 5-10 % for all the outputs that can be made possible by rectifying the model limitations and errors.

As can be seen from the comparison of simulation and experimental results, there is a difference between two. There are a number of reasons for the error. Firstly, the assumptions made for the wind turbine model in the simulation, result in an approximation of the torque model for the Savonius rotor. Secondly, the PMSG parameters in the simulation vary from the PMSG used in the experimental system the parameters for the PMSG used in experimental system are unknown. Thirdly, the mathematical model does not include any three-dimensional (3D) fluid effects, environmental effects, and the power loss through the vent between the rotor blades. The experimental system generates a very low power due to several reasons. First reason is the high instability of the turbine rotor due to the heavy weight. Second, the preventive net further reduces the efficiency of the turbine by reducing the net force acting on the rotor. Third, the wheels used for maintaining mobility of the wind turbine add to the instability of the system as the system keep vibrating and displacing hence, preventing the rotor from reaching a stable rpm.

# CHAPTER SEVEN

# CONCLUSION

The work in this thesis presents a complete model of a Savonius wind turbine. An approximate lumped parameter model for the wind turbine system was developed using the mathematical equations for the torque acting on the Savonius rotor as per Appendix C. There are a number of assumptions made in the torque calculations i.e. the wind force acting on the rotor surface remains constant the entire time, the coefficient of drag does not vary with the rotation, and the rotor area exposed to the wind remains constant. Also, the three dimensional fluid effects are ignored to further simplify the formulation of torque formula. The PMSG model is developed using the simplified equations in the d-q synchronous rotating reference frame. The entire wind turbine system is implemented in the MATLAB/Simulink environment to study the system response under different wind speeds. The wind turbine parameters used in the simulation are per Table D.3 and the PMSG parameters used are per Table D.3 (Khater *et al.*, 1978). The results from the experimental setup were obtained using the National Instruments Data Acquisition Device. The outputs from the sensors and the transducers are connected to the NI DAQ device. For real time data acquisition process a program has been generated in the LabView software. The experimental and simulation data has been exported to Excel for further analysis and comparison.

A comparison of the experimental and numerical results shows some differences which may be attributed to the fact that the mathematical model developed for torque acting on the Savonius rotor. An approximate model for the torque has been developed as per

Appendix B. The model does not account for the three-dimensional (3D) fluid effects and environmental effects. Also, an assumptions has been made for the PMSG parameters used in the simulation (refer to Table D.3) because the PMSG parameters are unknown for the experimental system. Considering the size of the experimental Savonius wind turbine, the electrical power generated is very low. There are a number of reasons for the low electrical power generation. First, the thickness of the aluminum sheet used for the rotor buckets is large and results in high system inertia. Also, the wooden end plates further add to the inertia of the system. Second, the misalignment of the rotor buckets attached to the shaft leads to instability of the turbine rotor. Third, the protective wire mesh around the frame of the turbine reduces the effective wind force acting on the wind turbine rotor. Fourth, the wheels added to the frame for the purpose of mobility of the wind turbine, reduce the stability of the system. All of the above reasons reduce the rotor speed, therefore reducing the power generated by the wind turbine.

# APPENDICES

# Appendix A

## MATLAB Code

Torque Calculation

```
A_t = D_t*H_t;          % area of turbine rotor (m^2)

B = 0.0065;             % damping coefficient

Cd1 = 2.3;              % coefficient of drag of advancing side

Cd2 = 1.1;              % coefficient of drag of retreating side

D_t = 0.7112;           % diameter of turbine rotor (m)

H_s = 1.20015;          % height of the shaft (m)

H_t = 0.5842;           % height of the turbine rotor (m)

J = (4*rho2*H_t*t_t*r_t^3/3) + ((2*pi*r_s*H_s + 2*pi*r_s^2)*rho2*r_s^2/2)+

(rho3*pi*r_p^4*t_p);    % moment of inertia

Jg = 0.026;             % moment of inertia of generator

Je = Jg + J;            % total moment of inertia

rho1 = 1.2754;          % density of air (kg/m^3)

rho2 = 2700;            % density of aluminum (kg/m^3)

rho3 = 600;             % density of plywood (kg/m^3)

r_p = 0.4064;           % radius of end plate (m)

r_s = 0.0127;           % radius of the shaft (m)

r_t= d_t/2;             % radius of turbine rotor (m)

t_p = 0.0127;           % thickness of end plate (m)
```

```
t_t = 0.00762;            % thickness of turbine rotor (m)


% torque calculation
k=1;
X = 0.5*A_t*rho1*(Cd1-Cd2)*d_t;          % constant terms in the torque integral
syms x
for a=0:pi/60:2*pi                       % angle of attack varies from 0 to 2*pi
    q = int(cos(x)*sin((a+x)) , x, 0, pi/2);     % integral varying theta from 0 to pi/2
    Q = abs(q);                          % absolute value of the torque
    torque(k,1)= Q;
    k = k+1;
    plot(a*180/pi,Q,'*')                 % plotting torque vs angle of attack
    hold on
end
W = double(torque);
hold off
```

## Appendix B

## Torque Calculation for Savonius Rotor

A mathematical model for the torque acting on the Savonius rotor is derived using the formula, *Torque* = *Force* x *Distance*.

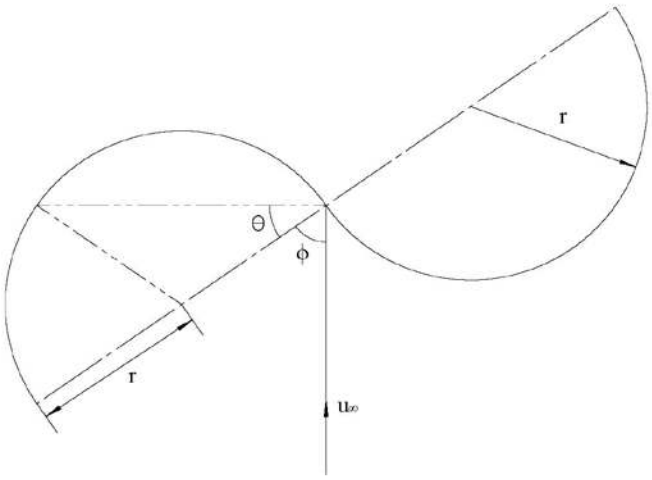


Figure B.1: Savonius Rotor Schematic.

In Figure B.1, α is the angle of attack, $\theta$ is the angle subtended by the point of impact at the center of the rotor, $r$ is the radius of the semi-circular section of the rotor, and $u_\infty$ is the free stream velocity.

1. Given : $r$, $\theta$, $\alpha$, $A$ (area of rotor), $\rho$ (free stream density), $C_d$ (Coefficient of drag), $u_\infty$, and $F$ (wind force)

$$F = \frac{1}{2}\rho A u_\infty^2 C_d \tag{B.1}$$

2. According to the definition: *Torque* = *Force* x *Distance*

From figure B.2, we can deduce that

$$T = OA \times F = OA.F.\sin(\angle \mathrm{OAC}) \tag{B.2}$$

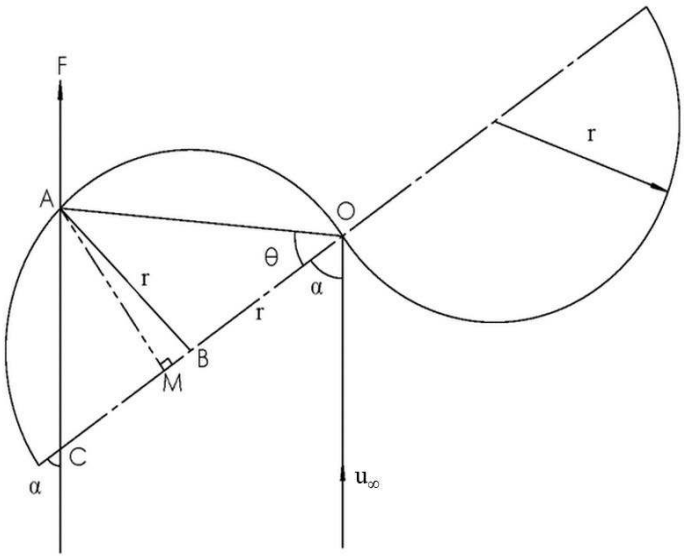


Figure B.2: Savonius Rotor with Angles and Forces.

3. *In* ΔAMB,

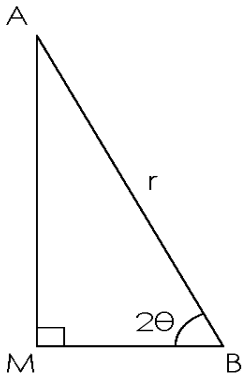


Figure B.3: Calculating the Length, MB.

- Case I (when $2\Theta < \pi/2$)

$$-\cos(2\theta) = \frac{MB}{r} \tag{B.3}$$

$$So, MB = -r\cos(2\theta) \tag{B.4}$$

- Case II (when $2\Theta > \pi/2$)

$$-\cos(2\theta) = \frac{MB}{r} \tag{B.5}$$

$$So, MB = -r\cos(2\theta) \tag{B.6}$$

4. *In* ΔAMO *and* ΔABO,

- Case I

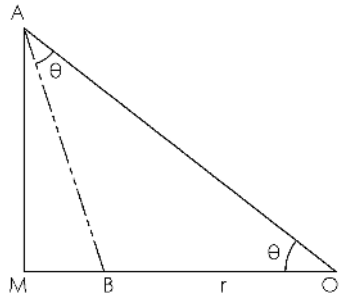


Figure B.4: Calculating the Length, OM.

$$OM = OB + BM \tag{B.7}$$

$$OM = r + r\cos(2\theta) = \mathrm{r}(1+\cos(2\theta)) \tag{B.8}$$

- Case II

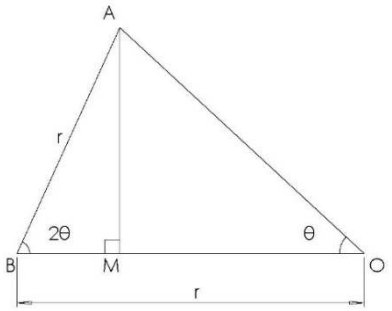


Figure B.5: Calculating the Length, OA.

$$OM = OB - BM \tag{B.9}$$

$$OM = r + r\cos(2\theta) = \mathrm{r}(1+\cos(2\theta)) \tag{B.10}$$

$$Also,\ \cos(\theta) = \frac{OM}{OA} \tag{B.11}$$

$$OA = \frac{OM}{\cos(\theta)} \tag{B.12}$$

$$OA = \frac{r(1+\cos(2\theta))}{\cos(\theta)} = \frac{r(1+2\cos^2\theta - 1)}{\cos(\theta)} = 2r\cos\theta \tag{B.13}$$

5. *In* ΔOAC,

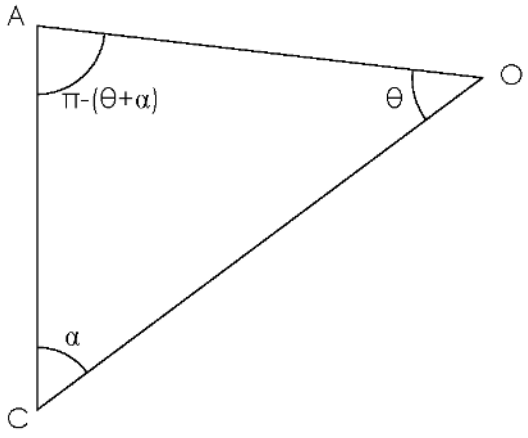


Figure B.6: Calculating the Angle, OAC.

$$\angle \text{OAC} = (\pi - (\theta+\alpha)) \tag{B.14}$$

6. Substituting the unknowns into the equation of torque gives ;

$$T = OA.F.\sin(\angle OAC) \tag{B.15}$$

$$T = 2r\cos\theta\left(\frac{1}{2}A\rho u_\infty^2 C_d\right)\sin(\pi-(\theta+\alpha)) \tag{B.16}$$

$$T = 2r\cos\theta\left(\frac{1}{2}A\rho u_\infty^2 C_d\right)\sin(\theta+\alpha) \tag{B.17}$$

Net torque on the rotor is given by

$$T_{net} = \int_0^{\pi/2} 2r\cos\theta\left(\frac{1}{2}\rho u_\infty^2 C_d\right)\sin(\theta+\alpha)d\theta \tag{B.18}$$

$$T_{net} = \left(A\rho u_\infty^2 C_d\right)\int_0^{\pi/2}\left(r\cos\theta\right)\sin(\theta+\alpha)d\theta \tag{B.19}$$

where $\alpha$ varies from 0 to $2\pi$.

# Appendix C

## Lookup Plots

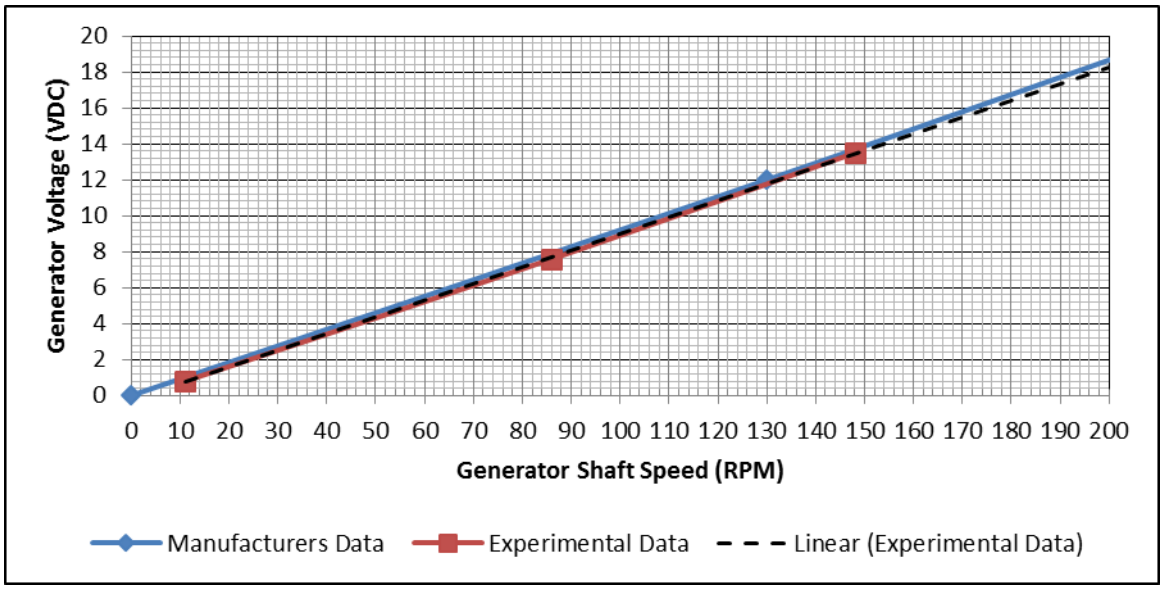


Figure C.1: Manufacturer's Plots Validation (No Load Voltage).

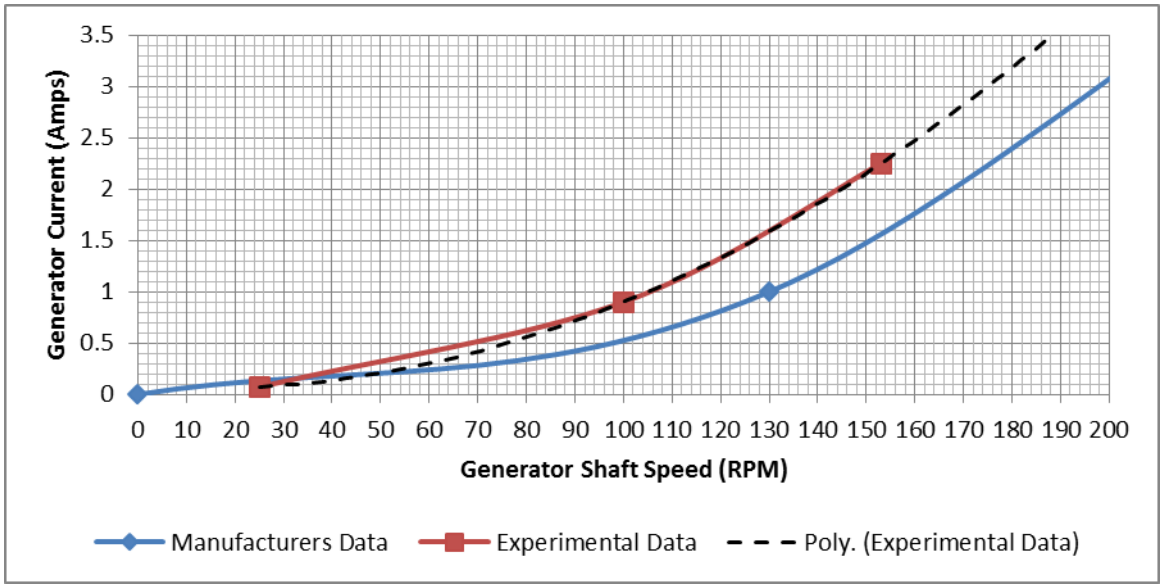


Figure C.2: Manufacturer's Plots Validation (Short Circuit Current).

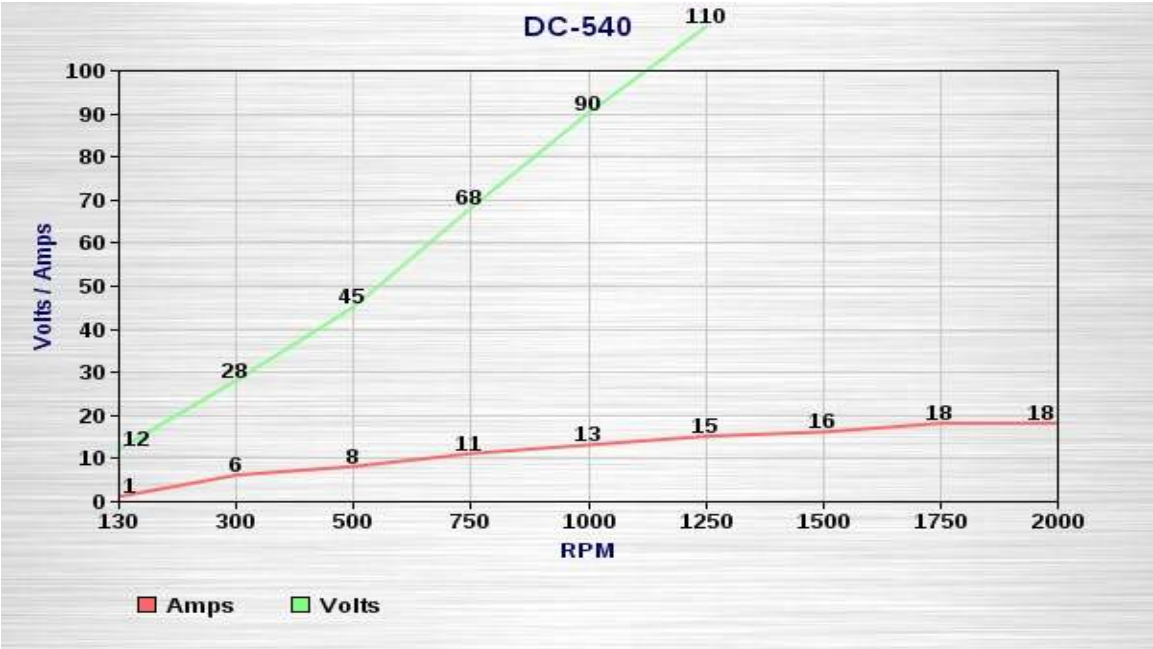


Figure C.3: Manufacturer's Plot for No Load Voltage and Short-circuit Current.

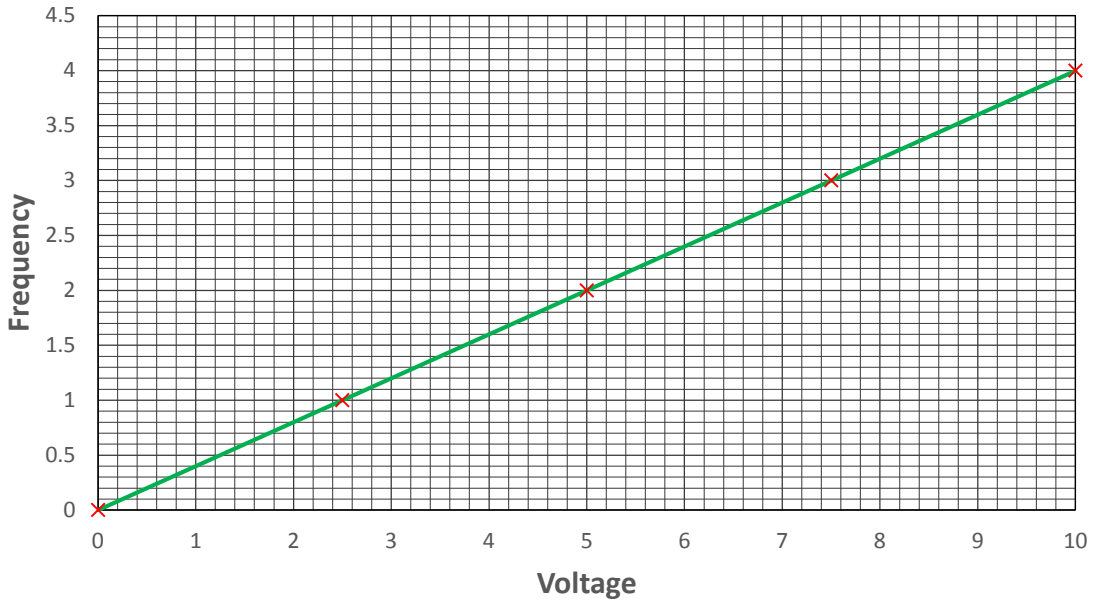


Figure C.4: Lookup Plot for Rotor RPM.

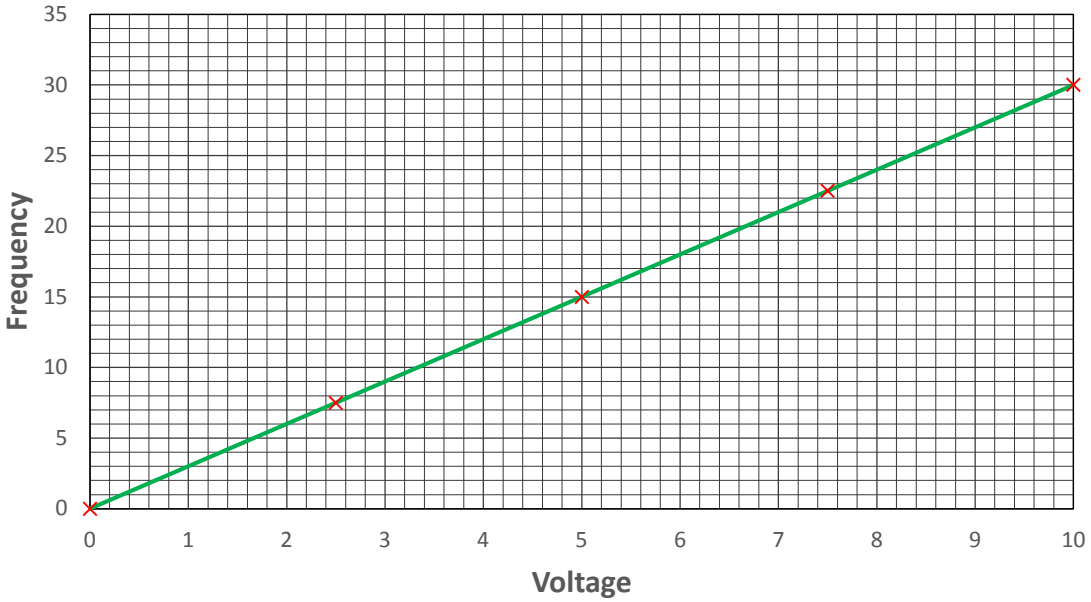


Figure C.5: Lookup Plot for Anemometer RPM.

## Appendix D

## List of Materials and Components

Table D.1: List of Materials.

| **Materials** | **Dimensions** | |
|---|---|---|
| Aluminum sheet | Thickness = 0.0076 m | Length = 1.12 m, Width = 0.58 m |
| Bearings | Quantity = 2 | |
| Extruded aluminum frame | Length = 13.10 m | Height = 0.0254 m |
| Shaft | Length = 1.20 m | Diameter = 0.0254 m |
| Stainless steel net | Length = 1.092 m | Height = 1.175 m |
| Wooden sheet | Thickness = 0.0127 m | Diameter = 0.82 m |

Table D.2: List of Components.

| **Part** | **Manufacturer** | **Part Number** | **Specs** |
|---|---|---|---|
| Alternator | Wind Blue | DC 540 | 3 phase AC |
| Blower | Triple S | Mach III | 1 HP, 4100 CFM, 110 VAC |
| Current Transducer | CR Magnetics | CR5200-2 | 0-2 ADC, 0-5 VDC, 24 VDC |
| DAQ card (ADC) | National Instruments | USB 6001 | USB powered |
| Frequency to Analog Converter (Quantity = 2) | Red Lion Controls | IFMA0035 | 1 Hz - 25 kHz, 0-10VDC, 24 VDC |
| Power Supply | CR Magnetics | CRPS24VDC-120 | 24 VDC, 110 VAC |
| Proximity Sensor 1 | Square D | Class 9006 Type PJA112N | 9-32 VDC |
| Proximity Sensor 2 | Square D | Class 9006 Type PJD112N | 9-32 VDC |
| Rectifier | Misol | WDT-FW-1203-1 | 300 W 12, 15 V Brake Voltage |
| Voltage Transducer | CR Magnetics | CR5310-50 | 0-50 VDC ,0-5 VDC, 24 VDC |

Table D.3: Summary of Model Parameters with Numerical Values and Corresponding Units.

| Symbol | Parameter | Value | Units |
|---|---|---|---|
| A | Swept Area | 0.4155 | $m^2$ |
| B | Damping Coefficient | 0.3 | - |
| D | Rotor Diameter | 0.7112 | m |
| $D_o$ | End Plate Diameter | 0.8128 | m |
| $f$ | Frequency | 36 | Hz |
| H | Rotor Height | 0.5842 | m |
| $J_g$ | Generator Inertia | 3.1053 | $kgm^2$ |
| $L_d = L_q$ | d-q axis Inductance | 5.0 | mH |
| n | Number of Blades | 2 | - |
| P | Pole Pairs | 12 | - |
| $P_{base}$ | Rated Power | 1000 | W |
| $R_s$ | Stator Resistance | 20 | Ohm |
| $T_{base}$ | Rated Torque | 35.37 | Nm |
| $t_p$ | Thickness of End Plate | 0.0127 | m |
| $t_t$ | Thickness of Rotor | 0.0076 | m |
| $V_{base}$ | $Voltage_{Line-Line}$ | 165 | V |
| $\omega_{base}$ | Rated Speed | 28.27 | rad/sec |
| $\lambda_r$ | Flux | 0.60 | Wb |
| $\eta_{gen}$ | Generator Efficiency | 33% | - |
| $\eta_{mech}$ | Mechanical Efficiency | 70% | - |

The following equation have been used in calculating the base values of parameters for per-unit (pu) system conversion. The dynamic equations of the PMSG have been simulated in per-unit system and the results are converted to absolute values using the following equations.

$$P_{base} = T_{base}\omega_{base} \tag{D.1}$$

$$I_{base} = \frac{P_{base}}{\sqrt{3} \times V_{base}} \; ; \; V_{base} = V_{L-L} \tag{D.2}$$

$$Z_{base} = \frac{V_{base}}{\sqrt{3} \times I_{base}} \tag{D.3}$$

$$\lambda_{r_{base}} = L_{base} I_{base} \tag{D.4}$$

$$L_{d,q_{pu}} = \frac{L_{d,q}}{L_{base}} \tag{D.5}$$

$$R_{s_{pu}} = \frac{R_s}{Z_{base}} \tag{D.6}$$

$$L_{base} = \frac{Z_{base}}{2\pi f} \tag{D.7}$$

For instance, consider the case where the base voltage (line-line), $V_{base}$, and the base current, $I_{base}$, are 165 V and 3.5 A, respectively for a 1 kW generator (refer to Table D.3). The base impedance, $Z_{base}$, and the base inductance, $L_{base}$, can be calculated as

$$Z_{base} = \frac{V_{base}}{\sqrt{3} \times I_{base}} = \frac{165}{\sqrt{3} \times 3.5} = 27.22 \tag{D.8}$$

$$L_{base} = \frac{Z_{base}}{2\pi f} = \frac{27.22}{2\pi(36)} = 0.1204 \tag{D.9}$$

assuming a frequency of 36 Hz for the selected generator (refer to Table III). Therefore, the *d*- and *q*- axis inductances in per-unit (pu), $L_{d,q\ pu}$, can be calculated if $L_{d,q}$, = 0.005 H as

$$L_{d,q_{pu}} = \frac{L_{d,q}}{L_{base}} = \frac{0.005}{0.1204} = 0.0415 \tag{D.10}$$

# REFERENCES


Ahmed, A. A., Abdel-Latif, K. M., Eissa, M. M., Wasfy, S. M., and Malik O.P., "Study of Characteristics of Wind Turbine PMSG With Reduced Switches Count Converters", *IEEE Canadian Conference of Electrical and Computer Engineering*, pp. 1-5, Regina, SK, 2013.

Akwa, J. V., Vielmo, H. A., and Petry, A. P., "A Review on the Performance of Savonius Wind Turbines", *Renewable and Sustainable Energy Reviews*, vol. 16, no. 5, pp. 3054–3064, 2012.

Ali, G., Wagner, J., Moline, D., and Schweisinger, T., "Energy Harvesting from Atmospheric Variations - Theory and Test", *Renewable Energy*, vol. 74, no. C, pp. 528-535, 2015.

Ali, M., "Experimental Comparison Study for Savonius Wind Turbine of Two & Three Blades At Low Wind Speed", *International Journal of Modern Engineering Research*, vol. 3, no. 5, pp. 2978–2986, 2013.

Altan, B. D., and Atilgan, M., "An Experimental and Numerical Study on the Improvement of the Performance of Savonius Wind Rotor", *Energy Conversion and Management*, vol. 49, no. 12, pp. 3425–3432, 2008.

Badoni, P., and Prakash, S. B., "Modeling and Simulation of 2 MW PMSG Wind Energy Conversion Systems", *IOSR Journal of Electrical and Electronics Engineering*, vol. 9, no. 4, ver. 1, pp. 53-58, 2014.

British Petroleum, "BP Statistical Review of World Energy June 2015", https://www.bp.com/content/dam/bp/pdf/energy-economics/statistical-review-2015/bp-statistical-review-of-world-energy-2015-full-report.pdf, Accessed Feb 2016.

Cultura II, A. B., and Salameh, Z. M., "Modeling and Simulation of a Wind Turbine-Generator System", *IEEE Power and Energy Society General Meeting*, pp. 1-7, San Diego, CA, 2011.

D'Alessandro, V., Montelpare, S., Ricci, R., and Secchiaroli, A., "Unsteady Aerodynamics of a Savonius Wind Rotor: A New Computational Approach for the Simulation of Energy Performance", *Energy*, vol. 35, no. 8, pp. 3349–3363, 2010.

Deb, B., Gupta, R., and Misra, R. D., "Performance Analysis of a Helical Savonius Rotor Without Shaft at 45 Twist Angle Using CFD", *Journal of Urban and Environmental Engineering*, vol.7, no. 1, pp. 126–133, 2013.

Elbeji, O., Hamed, M. B., and Sbita, S., "PMSG Wind Energy Conversion System: Modeling and Control", *International Journal of Modern Nonlinear Theory and Application*, vol. 3, no. 3, pp. 88-97, 2014.

El-Askary, W. A., Nasef, M. H., AbdEL-hamid, A. A., Gad, H. E., "Harvesting Wind Energy for Improving Performance of Savonius Rotor", *Journal of Wind Engineering and Industrial Aerodynamics*, vol. 139, pp. 8-15, 2015.

El-Saady, G., Ibrahim, E. N. A., Ziedan, H., & Soliman, M. M., "Analysis of Wind Turbine Driven Permanent Magnet Synchronous Generator under Different Loading Conditions", *Innovative Systems Design and Engineering*, vol. 4, no. 14, pp. 97-111, 2013.

Farsaie, A., Smith, G. L., and Brill, B., "Evaluation of a Horizontal Savonius", *Transactions of the American Society of Agricultural Engineers,* vol. 27, no.1, pp. 241-244, 1984.

Fujisawa, N., and Gotoh, F., "Pressure Measurements and Flow Visualization of a Savonius Rotor", *Journal of Wind Engineering and Industrial Aerodynamics*, vol. 39, no. 1-3, pp. 51–60, 1992.

Global Wind Energy Council, "Global Wind Statistics 2015",http://www.gwec.net/wp-content/uploads/vip/GWEC-PRstats-2015_LR_corrected.pdf, Accessed 2016.

Gupta, J., and Kumar, A., "Fixed Pitch Wind Turbine-Based Permanent Magnet Synchronous Machine Model for Wind Energy Conversion Systems", *Journal of Engineering and Technology*, vol. 2, no. 1, pp. 52-62, 2012.

Hassan, I., Iqbal, T., Khan, N., Hinchey, M., and Masek, V., "CFD Analysis of a Twisted Savonius Turbine", *Renewable Energy*, vol. 4, pp. 3–6, 2010.

Hayashi, T., Li, Y., and Hara, Y., "Wind Tunnel Tests on a Different Phase Three-Stage Savonius Rotor", *JSME International Journal Series B*, vol. 48, no. 1, pp. 9–16, 2005.

Kamoji, M. A., Kedare, S. B., and Prabhu, S. V., "Experimental Investigations on Single Stage, Two Stage and Three Stage Conventional Savonius Rotor", *International Journal of Energy Research*, vol. 32, no. 10, pp. 877–895, 2008.

Khan, M. H., "Model and Prototype Performance Characteristics of Savonius Rotor Windmill", *Wind Engineering*, vol. 2, no. 2, pp. 75–85, 1978.

Khater, F., Shaltout, A., and Omar, A., "Control of Direct Driven PMSG for Wind Energy System", *Latest Trends on Systems*, vol. 2, no. 2, pp. 455-461, 2014.

Koch-Ciobotaru, C., "Data Acquisition System for a Vertical Axis Wind Turbine Prototype", *Selected Topics in Energy, Environment, Sustainable Development and Landscaping. Ministry of Labour, Family and Social Protection*, Romania, 2009.

Lu, X., McElroy, M. B., and Kiviluoma, J., "Global potential for wind-generated electricity", *proceeding of the National Academy of Sciences of the United States of America*, vol. 106, no. 27, pp. 10933-10938, 2009.

Modi, V. J., and Fernando, M. S. U. K., "On the Performance of Savonius Wind Turbine", *Journal of Solar Energy Engineering*, vol. 111, no. 1, pp. 71–81, 1989.

Rahman, M., Morshed, K. N., Lewis, J., and Fuller, M., "Experimental and numerical investigations on drag and torque characteristics of three-bladed Savonius wind turbine", *International Mechanical Engineering Congress and Exposition*, ASME, vol. 6, pp. 85-94, 2009.

Saha, U. K., and Rajkumar, M. J., "On the Performance Analysis of Savonius Rotor with Twisted Blades", *Renewable Energy*, vol. 31, no. 11, pp. 1776–1788, 2006.

Saha, U. K., Thotla, S., and Maity, D., "Optimum Design Configuration of Savonius Rotor Through Wind Tunnel Experiments", *Journal of Wind Engineering and Industrial Aerodynamics,* vol. 96, no. 8-9, pp. 1359–1375, 2008.

Sankar, A. B., and Seyezhai, R., "MATLAB Simulation for Power Electronic Converter for PMSG Based Wind Energy Conversion System", *International Journal of Innovative Research in Electical, Electronics, Instrumentation and Control Engineering,* vol. 1, no.9, pp. 348-353, 2013.

Sharma, K. K., Gupta, R., Singh, S. K., and Singh, S. R., "Experimental investigation of the characteristics of a Savonius wind turbine", *Wind Engineering,* vol. 29, no.1, pp. 77-82, 2005.

Wakui, T., Tanzawa, Y., Hashizume, T., and Nagao, T., "Hybrid Configuration of Darrieus and Savonius Rotors for Stand-alone Wind Turbine-Generator Systems", *Electrical Engineering in Japan*, vol. 150, no. 4, pp. 13–22, 2013.

Weisgerber, S., Proca, A., and Keyhani, A., "Estimation of Permanent Magnet Motor Parameters", *IEEE Industry Application Society Annual Meeting*, vol. 1, pp. 29-34, New Orleans, LA, 1997.

Wind Blue Power, "Permanent Magnet Alternator Model DC 540", http://www.windblue-power.com/Permanent_Magnet_Alternator_Wind_Blue_Low_Wind_p/dc-540.htm, Accessed June 2015.

Wind Energy Foundation, “History of Wind Energy”, http://windenergyfoundation.org/about-wind-energy/history/, Accessed Feb 2016.

Yin, M., Li, G., Zhou, M., and Zhao, C., "Modeling of the Wind Turbine with a Permanent Magnet Synchronous Generator for Integration", *IEEE Power Energy Society General Meeting*, pp. 1-6, Tampa, FL, 2007.